29452 DUP

IGM88TC-108-774-G
CNRC 29452

MELT FLOW OF POLYETHYLENE BLENDS

L.A. Utracki

Conseil national de recherches du Canada
Institut de génie des matériaux
75, De Mortagne
Boucherville, Québec, Canada J4B 6Y4,
Tel. (514) 641-2280, telex 055-61622

The rheology of polyethylene blends is discussed with an emphasis on those containing the linear low density polyethylenes, LLDPE. Flow of LLDPE with other types of LLDPE's, with low density polyethylene, LDPE, and with polypropylene, PP, was studied in steady state shear, dynamic shear and uniaxial extensional fields. Interrelations between diverse rheological functions are discussed in terms of the linear viscoelastic behavior and its modification by phase separation into complex morphology. One of the more important observations is the difference in elongational flow behavior of LLDPE/PP blends from that of the other blends; the strain hardening (important for e.g. film blowing and wire coating) occurs in the latter ones but not in the former.

Polyethylenes, PE, constitute an important part of the plastics market (see Table I). Since their discovery in 1933 they have seen continuous rise in consumption to the present level of 25 M tons per annum, or 42% of all plastics (1). This extended period of growth originates in continuous development and modification of these resins, resulting from a widening range of polymerization techniques.

The history of PE can be divided into three periods: 1. the initial, characterized by predominence of the radical polymerization of ethylene, C_2, at high temperature and pressure, 2. development of coordination copolymerization of C_2 with other α-olefins, and 3. development of polymer blending technology. It is interesting that new methods have been developed without the older ones becoming obsolete. Thus it is difficult to put firm dates on transitions between these three periods. Development of Ziggler-Natta catalysts resulted in commercialization of high density polyethylene, HDPE, which had to be "toughened" by copolymerization with butene, C_4. Next was development of the linear low density polyethylenes, LLDPE, by DuPont Canada in the late 1950's. The polymer was prepared by coordination polymerization in solution of C_2 with 10 to 20 mol% of C_4, C_6 or C_8. In 1979 Union Carbide patented the gas phase fluodized

bed polymerization process. It not only made LLDPE more popular around the world but also led to an ingress of blending methods as well as to development of new PE copolymers with very low density, butene based, VLDPE, and ultra low density, octene based, ULDPE. Both VLDPE and ULDPE are basically LLDPE copolymers with low crystallinity.

It is estimated that 60 to 70% LLDPE (including VLDPE and ULDPE) enters the market as blends. One may distinguish several categories of PE-blends.

(i) PE blends with a small quantity of "external lubricant": fluoro-polymers, siloxanes, PE-waxes, etc. These blends are primarily formulated for improvement of processability without affecting the PE performance (2).

(ii) PE blends with high concentration of rigid polymer. To this category belong blends of engineering resins with up to 10% of non-compatibilized PE acting as a toughening agent. Development of PE-ionomers and maleated PE allows for increase of PE content, generating a new class of materials.

(iii) PE blends with up to 30 wt% of a rigid polymer. The additional polymer plays the filler role increasing both the modulus and the heat deflection temperature. At low concentration, say below 5% of rigid polymer, the compatibilization is seldom necessary, but it is a must for blends at higher loadings.

(iv) LLDPE blends with other polyolefins or elastomers. These blends are mainly designed for improved processability via increase of the melt strength in film blowing or wire coating applications.

(v) PE blends with polypropylene, PP, and/or with one of their copolymers, EPR, EPDM, etc. constitute a large and important segment of the plastics market.

In this chapter only blends (iv) and (v) will be discussed.

LITERATURE SURVEY

The methods of PE polymerization and characterization of PE structures can be found in recent publications (3-6). The melt flow of PE's and their blends has been reviewed by Plochocki (7-9) and Utracki (10, 11). In the following text, recent information on PE/PE and PE/PP melt rheology will be outlined.

Polyethylene/Polyethylene Blends

Since the homologous polymer blends are known to be miscible it is not surprising that mixtures of **HDPE** with **HDPE** or **LDPE** with **LDPE** are miscible as well (12, 13). However, due to the diversity of polymerization methods and the variety of resulting molecular characteristics **LLDPE/LLDPE** systems are not always miscible (10, 14-15). In our laboratory three series of blends were prepared by identical procedures of mixing the same LLDPE with two other LLDPE resins and with LDPE. The zero-shear viscosity vs. composition dependence, η vs. w_2, of these systems is presented in Fig. 1. Only the LLDPE's prepared with the same Ti-catalyst were found to be miscible (curve 2). Neither blend of LLDPE with LDPE (curve 3) nor LLDPE prepared with a vanadium catalyst LLDPE (curve 1) were

miscible. There are indications in the literature (8) that variations of η_0 with composition such as shown in Fig. 1 are a reflection of similar density changes caused by the thermodynamic interactions.

Dumoulin et al. (16) studied morphology and properties of HDPE blended with another HDPE resin of nearly identical density but ten times higher molecular weight. The melt-blending was carried out by three different methods. The polymers were found to be immiscible; the ultra high molecular weight component, UHMWPE, partially dissolved in the normal molecular weight (Mw = 280 kg/mole) polymer with the rest behaving as reinforcing filler particles. These observations were confirmed by Vadhar and Kyu (17) who concluded that only by dissolving UHMWPE and LLDPE in a common solvent, then casting, could the uniform, miscible blends be obtained.

Since dissolution of UHMWPE strongly affects the molecular weight distribution, MWD, of the matrix polymer, any rheological function sensitive to MWD can be used to follow the dissolution process. The dynamic viscoelastic data provided a simple and easy tool (10, 11). As will be discussed later, to accomplish this the dynamic data were examined using either: (i) Zeichner-Patel cross-point coordinates, (ii) Cole-Cole plot, or (iii) the relaxation spectrum. The stress growth or relaxation functions in shear or extension depend on MWD as well. These were also used in studies of blend miscibility by rheological means (11).

Use of rheological functions for detecting the state of PE-blend miscibility in the melt is particularly attractive. The only other available method is the direct and costly, Small Angle Neutron Scattering, SANS (18). The latter method requires deuteration of one component which may affect miscibility (19). All available information on miscibility of PE blends indicates that in the absence of strong thermodynamic interactions both the dissolution and the phase separation are diffusion controlled. Frequently, one can generate homogeneous melt via dissolution in a common solvent (20) while the melt blending will result in a phase-separated material. There is direct evidence of true miscibility in homologous polymer blends, while even a small change in polymerization method, polymer composition or structure may lead to apparent immiscibility (14, 15). Since for the high molecular weight, industrial PE the conformational entropy of mixing is negligibly small and there are no specific interactions between two polyethylenes of different structure, one can appreciate that in these systems the miscibility is controlled by small departures from zero of the free energy of mixing.

Blends of HDPE with LDPE were studied by Dobrescu (12) by means of a capillary viscometer. The constant stress viscosity, log $\eta(\sigma_{12}=\text{const})$ vs. w_2 plot indicated a strong positive deviation, PDB, from the log-additivity rule:

$$\log \eta = \sum w_i \log \eta_i \qquad (1)$$

where $\eta = \eta(\sigma_{12})$ is the constant stress viscosity of the blend and η_i, $i = 1, 2$ that of the components. The blends were reported immiscible. The higher the viscosity ratio η_i/η_j, the larger was

the PDB deviation. Kammer and Socher (21) studied the two-phase HDPE/LDPE blends using the cone-and-plate, steady state rotational rheometer. Plots of the zero shear viscosity, η_0, the first normal stress difference coefficient ψ_{10} and the principal relaxation time, τ vs. w_2, all indicated PDB. In spite of immiscibility the shear viscosity data in a temperature range from 160 to 200°C could be superimposed on a master curve (22, 23):

$$\eta/\eta_0 = f(\dot{\gamma}\eta_0/T) \tag{2}$$

The compositional dependence of both $\eta = \eta(\sigma_{12})$ and the extrudate swell, $B = B(\sigma_{12})$ was PDB type. In conclusion, the current rheological information consistently reports that HDPE/LDPE systems are immiscible.

Santamaria and White (24) studied melt flow behavior and spinnability of several polyolefin systems including HDPE/LDPE blends. Defining the steady state compliance as:

$$J_e = N_1/2\sigma_{12}^2 \tag{3}$$

where N_1 is the first normal stress difference and σ_{12} the shear stress, the authors observed that J_e vs. w_2 shows a strong negative deviation from additivity. Furthermore, the extrudate shrinkage was nearly constant, independent of composition. Since the critical drawdown ratio was a linear function of the shrinkage, the net spinnability of HDPE and its blends with LDPE was low. The phase morphology was not studied.

The most important commercial blends of PE are those of **LLDPE with LDPE** (25, 26). The capillary flow data $\eta = \eta(\sigma_{12})$ and $B = B(\sigma_{12})$, indicated (similar to HDPE/LDPE) PDB-type behavior (27-29). The latter authors also reported a PDB relation between melt strength and composition. Recently (14, 15) these blends were studied under the steady state and dynamic shear flow as well as in uniaxial extension. A more detailed review of these results will be given in part 3 of this chapter. Like HDPE/LDPE blends, those of LLDPE/LDPE type are also consistently reported as immiscible.

Polypropylene/Polyethylene blends

PP/PE blends are of major commercial interest. Patents on PP with HDPE, LDPE and more recently with LLDPE constitute well over 40% of all patents on polyolefin blends. The main reason for blending is improvement of: processibility, low temperature toughness and impact strength (PP with HDPE or LLDPE), film clarity, drawability, orientability (PP with LDPE), etc. (8). Some of these blends, especially those with LDPE, may require the addition of a compatibilizing copolymer, e.g. EPR or EPDM. The blends find application in automobiles, appliances, houseware, furniture, sporting goods, toys, packaging, chemical processing equipment and industrial components. The PE/PP systems are immiscible. Depending on the type and molecular parameters of the components the degree of immiscibility may be such that compatibilizing copolymers, viz. EPR, have to be added (8, 30, 31). The ultimate mechanical properties,

i.e. impact strength, the stress and maximum strain at break, are the most sensitive to the extent of compatibility.

The capillary viscosities of **HDPE/PP** systems at 180 to 210°C were reported (32, 33) to superimpose on the Equation 2 master curve, with η_0 following the Arrhenius dependence:

$$lu\ \eta_0 = A + E_\eta/RT \tag{4}$$

where A is a parameter, E_η the activation energy of flow and R the gas constant. The plot of shear viscosity at constant shear stress, $\eta = \eta(\sigma_{12})$, vs. volume fraction of the second component, ϕ_2, showed a negative deviation from the log additivity rule, Equation 2, NDB. Defining the viscosity ratio as:

$$\lambda = \eta_1/\eta_2 \tag{5}$$

where subscripts 1 and 2 represent the dispersed and the matrix phases respectively, the authors reported large differences in morphology for blends with $\lambda > 1$ and for those with $\lambda < 1$; in the first case the dispersed phase existed in a form of fibrillas, in the second as small droplets. The difference in structure originated in the kinetics of breakage of fibrillas created at the entrance to capillary. For systems whose $\lambda < 1$ the fluidity additivity equation (34) was found to be obeyed:

$$1/\eta = \beta_1 \sum w_i/\eta_i \tag{6}$$

with w_i replaced by ϕ_i and the slip coefficient $\beta_1 \approx 1$. For $\lambda > 1$ at concentrations $w_2 < 0.5$ Equation (1) yielded good approximation; at higher PP content, Equation 6 was obeyed.

The extrudate swell, $B = B(\sigma_{12})$, for HDPE and high PP-content blends, $w_2 \geq 0.75$, was independent of temperature. The plot for $w_2 = 0.25$ and 0.5 was temperature sensitive, indicating T-dependent morphology (32, 33). At high PP content and low strains the lower viscosity HDPE drops became deformed at the capillary entrance. Retraction of these fibers caused large extrudate swell. At high strains both phases were strained, yielding average, smaller B values. For high HDPE content the extrudate swell decreased with temperature, T, probably due to increased interlayer slip caused by lowering the viscosity.

Blends of three PP and two HDPE resins having different values of η_0 were studied in a capillary viscometer (35). Independently of the viscosity ratio, λ, at 200°C all blends showed small negative deviation from the log-additivity rule, NDB. The non-equilibrium extrudate swell (measured after quenching) at low stress showed small positive deviation from the additivity rule while at higher stresses the additivity. The NDB tendency for the viscosity combined with the constant critical shear stress for melt fracture, σ_{MF} = 2MPa, indicate a better extrudability of the PP/HDPE blends than that of the neat resins.

Blends of **PP with LDPE** have been of industrial interest for years (24, 35-38). Plots of $\eta = \eta(\sigma_{12})$ vs. w_2 invariably show NDB

(35, 36, 38) whose magnitude varies with the method of blend preparation (37) and stress level (24). The negative deviations indicate that the mechanism responsible for NDB is interlayer slip. According to Lin (34) the interlayer slip factor in Equation 6:

$$\beta_1 = 1 + (\beta_{12}/\sigma_{12})\ (w_1 w_2)^{1/2} \qquad (7)$$

where β_{12} is the characteristic slip factor of the blend, i.e. the NDB should be, as observed, more pronounced at small σ_{12}. The extrudate shrinkage was also reported (24, 38). Blends with $\lambda \approx 1$ were extruded, then placed in an oil bath at 190°C for about one hour. The shrinkage was calculated as

$$\varepsilon_\infty = \ln (L_0/L_\infty) \qquad (8)$$

where L_0 and L_∞ indicate the initial and final extrudate lengths, respectively. The plot of ε_∞ vs. composition is presented in Fig. 2. It can be shown that while the absolute magnitude of ε_∞ depends on the initial aspect ratio of the extrudate, the form of ε_∞ vs. w_2 does not. It is apparent that for the system with $\lambda \approx 1$ the maximum shrinkage occurs at $w_2 \approx 0.5$ where the fibrillation affects both co-continuous phases.

The flow properties of LLDPE/PP blends were studied by Dumoulin et al. (39-41). This subject will be discussed in the last part of this chapter.

Concluding the literature review the following remarks should be made: (i) the NDB behavior of $\eta = \eta(\sigma_{12})$ vs. w_2, a large extrudate shrinkage near $w_2 = 0.5$ and a sensitivity of the rheological functions to methods of blend preparation all indicate immiscibility (10, 11, 42, 43), (ii) the single phase flow of PE blends was reported only for homologous PE blends when the components' molecular weight $M_w < 10^6$ g/mole; the homologous HDPE/UHMWPE blend was found to form two phases, probably caused by the slow rate of UHMWPE dissolution in the mechanically compounded mixtures, (iii) blends of HDPE with LDPE were found to be immiscible, although the immiscibility may be marginal, disappearing at high temperatures for low molecular weight components, and (iv) blends of PE with PP show strong, nearly antagonistic immiscibility.

LLDPE Blends with PE

A standard commercial film blowing LLDPE resin, LPX-30, was blended at different ratios with either other LLDPE's or a LDPE polymer. The characteristic properties of these materials are listed in Table II. The resins were generously donated to the project by Esso Chem., Canada. Prior to blending the polymers were thoroughly characterized by SEC, SEC/LALLS, solution viscosity, ^{13}CNMR, Atomic Absorbance, and their rheological behavior was characterized in steady state and dynamic shear flow as well as in the uniaxial extensional deformation (44-46).

EXPERIMENTAL

Blending was done using a Werner-Pfleiderer co-rotating twin screw

extruder, model ZSK-30 at 140 rpm. The pelletized resins were pre-dry-blended and fed to the extruder using a volumetric metering feeder, Incrison model 105-C. The following temperature profile was used: (feeder) 158, 192, 214, 196 and (die) 196°C. The extrusion rate was Q = 6 to 8 kg/hr, indicating extensive backmixing. The extrudates were granulated, dried and formed into shapes suitable for rheological testing. The composition, code and molecular weight averages of the three types of blends are listed in Table III. Antioxydant, a mixture of Irganox 1010 and Irganox 1029, was used at a concentration 0.2 wt %.

For determination of the steady state shear viscosity the Instron capillary viscometer model 3211 was used at 190°C. Six capillaries were used, three each of diameter d = 747 and 1273 μm. The length to diameter ratio in each series varied from L/d = 0.6 to 60. The standard Bagley and Rabinowitsch corrections as well as that for the pressure effects (45) were applied. The extrudate swell was determined on air-cooled extrudates, 5 cm in length.

Rheometrics Mechanical Spectrometer, Model 605, RMS, was used in the dynamic mode at 150°C with the parallel plates geometry. To examine the thermal stability of the resins, first the two hours long time sweep at strain γ = 15% and frequency ω = 10 rads/s was carried out; the test samples were found to be stable for at least 60 min. The frequency sweep at γ = 15% was performed in two directions: for two samples from ω = 0.1 to 100 (rads/s) and for two others from 1 to 0.01 (rads/s). Two diameters of platens were used: 25 and 50 mm. The results were accepted if the maximum difference between the results of these four sweeps in the common range: ω = 0.1 to 1.0 did not differ by more than 5%. All tests were done under a blanket of dry nitrogen. The measurements were recorded using the RMS Columbia terminal, Model 964, then the data were transferred to a Hewlett-Packard, HP-85, mini-computer for analysis and mathematical manipulation, viz. calculation of two zero shear viscosities, η_0.

Rheometrics Extensional Rheometer, Model 605 (RER) was used at 150°C in a constant strain rate ($\dot{\varepsilon}$) mode. To facilitate storage and manipulation of data the RER was interfaced with a Hewlet-Packard model HP-85 micro-computer. For the test, the samples were transfer molded under vacuum, annealed, and then affixed with epoxy (24 hours curing) to the aluminum ties. Prepared in this manner, specimens did not show any shape change on immersion in hot (T = 150°C) silicone oil. The specimens were mounted in the instrument and immersed in Dow 200 silicon oil at 150°C. The test started after a 7 to 10 minute temperature equilibration period. During the measurements the maximum temperature difference, as read by three thermocouples placed at different heights in the sample chamber, did not exceed 0.5°C. For each sample the uniformity of the cylindrical shape was verified at three different heights; in all cases the average diameter was found to be d = 5.55 ± 0.05 mm. The sample length used in this study was L_0 = 22 mm ± 0.1 mm.

It is convenient to discuss results of this work under separate sub-titles, starting with the capillary, then with dynamic and finally the extensional flow behavior.

Pressure correction

It was observed that Bagley plots of pressure drop P vs. L/d were not always linear (45, 47):

$$P = \sum_{i=0}^{2} C_i \, (L/d)^i \tag{9}$$

It can be shown that parameters of Equation 9 are: $C_0 = P_e$ (the Bagley entrance and exit correction), $C_1 = 4\sigma_{12}$ and

$$C_2 = C_1^2 \, a_1 b_1 / 2P^* \tag{10}$$

where: a_1 is the temperature and pressure sensitivity parameter defined by the dependence:

$$\ln \eta_0 = a_0 + a_1/(f + a_2) \tag{11}$$

with f being the free volume fraction computed from the Simha-Somcynsky equation of state (48); b_1 is the free volume pressure coefficient defined by the relation:

$$1/f = b_0 + b_1 P/P^*; \text{ at } \tilde{T} \equiv T/T^* = \text{const.} \tag{12}$$

with P^* and T^* being characteristic (for a given liquid) pressure and temperature reducing factors, respectively. Note that according to Equation 12 $b_1 = b_1(\tilde{T})$ is a universal constant for all liquids at the reduced temperature $\tilde{T}$, i.e. both b_1 and P^* are determined by the thermodynamic properties of a system with only a_1 remaining unknown. For HDPE or LLDPE at 190°C, Equation 9 can be rearranged to:

$$a_1 = 154 \, \overline{(C_2/C_1^2)} \tag{13}$$

with the bar indicating the average value.

The values of a_1 were computed for a series of LLDPE and HDPE samples with a wide range of molecular weights. The data were found to follow the linear dependence:

$$a_1 = -0.1065 + 4031 \, M_w/M_n; \qquad M_w/M_n \leqslant 35 \tag{14}$$

with the correlation coefficient squared, $r^2 = 0.9945$.

Computation of a_1 resulted in the values plotted vs. composition in Fig. 3. According to Equation 14, a_1 depends on polydispersity which can be calculated from molecular weight averages of the neat polymers assuming their miscibility:

$$M_n^{-1} = \sum w_i / M_{ni} \tag{15}$$

$$M_w = \sum w_i M_{wi} \tag{16}$$

$$M_z = \sum w_i \, M_{zi} \, M_{wi} / \sum w_i \, M_{wi} \tag{17}$$

$$\therefore M_w/M_n = \sum(w_i/M_{ni}) \sum w_i M_{wi} \qquad (18)$$

The broken line in Figure 3 was computed from Equations 14 and 18 for blends of Series-I. The agreement between experimental results and the theoretical predictions based on ingredient miscibility confirms validity of the assumption. On the other hand, a_1 vs. LDPE content for blends of Series II show behavior incongruous with monotonic Equations 14 to 18 giving evidence of immiscibility. The extrema at II.20 and II.80 may indicate limits of miscibility. However, it is difficult to comprehend why crossing spinodals from the high LLDPE side results in a system with strong sensitivity of rheological behavior to T and P while crossing it from the high LDPE side generates blends with rheology insensitive to these independent variables.

Extrudate Swell

The extrudate swell, B = D/d, (where D and d are the extrudate and die diameter respectively) is plotted as B vs. w_2 in Fig. 4 for blends of Series I and II. In both cases B follows a simple parabolic equation:

$$B \equiv B_1 w_1 + B_2 w_2 + B_{12} w_1 w_2 \qquad (19)$$

with B_{12} = 0.32 ± 0.06 and 0.91 ± 0.05 for Series I and II respectively. The large B_{12} value for the latter blends suggests that here swelling is due to strain recovery of fibrillated drops rather than to extrudate swelling as in homologous polymer melts. Note that for system II the B vs. w_2 dependence resembles the extrudate shrinkage in Fig. 2.

Entrance flow

The entrance to capillary flow was studied by a flow visualization method (49). The flow pattern for Series II blends is presented in Fig. 5 (since the flow is axisymmetric only the left hand side part of the entrance region is shown). There is a large difference in flow pattern between that of LLDPE (0%) and of LDPE (100%). In the latter case the classical wine-glass shape with large vortices was observed. Upon a decrease of LDPE content both the glass-stem and vortices slowly decreased. It was noted that as little as 2% of LDPE was sufficient to introduce significant changes in LLDPE flow pattern. The mathematical modeling of the entrance flow allows correlation between the vortex size and the strain hardening in extensional flow.

The frequency dependence

The dynamic flow data can readily be evaluated in a three step process: (i) examination of the data for presence of an apparent yield stress, σ_y, and subsequently its subtraction, (ii) fitting the data to either the generalized Carreau model (42):

$$\eta' = G''(\omega)/\omega = \eta_0 \, [1+(\omega\tau_1)^{m_1}]^{-m_2} \qquad (20)$$

or to the Havriliak-Nagami dependence (50):

$$\eta^* \equiv G^*/\omega = \eta_0[1+(i\omega\tau_2)^{1-\alpha}]^{-\beta} \qquad (21)$$

and (iii) generalization of the results by deriving other linear viscoelastic dependencies by means of the intermediation of the Gross' frequency relaxation spectrum:

$$H_G(\omega) = \pm\,(1/\omega\pi)\mathrm{Im}G^*(\omega e^{\pm i\pi}) = (2/\omega\pi)\,\mathrm{Re}G''(\omega e^{\pm i\pi/2}) \qquad (22)$$

In Equations 20 to 22: η', η^* are dynamic and complex viscosity; G', G", G* are the storage, loss and complex shear modulus; ω is the frequency; τ_i the primary relaxation time; m_1, m_2, α, β are parameters: $i = \sqrt{-1}$; and Im, Re indicate the imaginary and real parts of the complex function, respectively.

The convenient way of data examination for presence of the apparent yield stress is by means of the modified Casson plot (51):

$$F^{\frac{1}{2}} = F_y^{\frac{1}{2}} + \underline{a}\,F_m^{\frac{1}{2}} \qquad (23)$$

where F, F_m and F_y are rheological functions of the blend, the matrix phase and its yield value, respectively; $\underline{a}$ is a parameter representing the square root of the relative F-function. For F any of these functions: σ_{12}, G', G", etc. can be used. The yield phenomenon originates in a stable three-dimensional structure. When the stress exceeds its yield value, $\sigma_{12} > \sigma_y$, the structure is destroyed and the material behavior changes from solid-like to liquid-like. In this classical description the rate is not considered. In blends at high concentration of dispersed phase the droplets either form interactive clusters or they coalesce into a co-continuous network (52, 53). The relaxation time of these interactive entities, τ_y, is rather long. When an experiment is carried out slowly enough, allowing the cluster to reform, $F_y \to 0$ can be found. On the other hand, when the experiment is conducted on a time scale comparable to τ_y, then the network response is analogous to that in the classical concept and $F_y \neq 0$ is observed. Formally one may express this idea in the form of the following relation:

$$F_y = F_y^{\infty}\,[1-\exp\{-\tau_y\omega\}] \qquad (24)$$

where τ_y is the relaxation time of interactive cluster. At a given frequency ω and when $\tau_y \to 0$ and ∞ the apparent yield stress $F_y = 0$ and $F_y = F_y^{\infty}$, respectively. Similarly for τ_y = const. (specific polymer blend) Fy reaches these limits for $\omega \to 0$ and $\omega \to \infty$. Experimental verification of dependencies 23 and 24 was recently published (52, 53). After the apparent yield stress is calculated, the experimental values, F_a, should be corrected by subtracting F_y:

$$F(\omega) = F_a(\omega) - F_y(\omega) \tag{25}$$

Once the values of $F(\omega)$ are known either Equation 20 or 21 can be used. The advantage of Equation 20 is that only $F_a = G''_a$ needs to be corrected for the apparent yield stress. If Equation 21 is to be used both G'_a and G''_a must be corrected independently and then:

$$G^* = (G'^2 + G''^2)^{\frac{1}{2}} \tag{26}$$

is calculated. (Note that since $G'_y \neq G''_y$ an attempt to use $F = G^*$ usually leads to nonsensical results).

Fig. 6 shows the curve-fit of η' vs. ω dependence for Series I and II blends by means of Equation 20. The fitting procedure generated the numerical values of the four parameters of the equation: η_0, τ, m_1 and m_2. It was found that the zero shear viscosity of homopolymers and blends followed the relation:

$$\eta_0 \propto M_\eta^a \tag{27}$$

where $a \simeq 3.5$. M_η, for polymers with log-normal distribution of molecular weights can be expressed as (45):

$$M_\eta = M_z(M_w/M_n)^{0.2} \tag{28}$$

The dependence is shown in Fig. 7.

From Equation 20 at $\omega \gg 1$ the power law exponent $n = 1 - m_1m_2$ i.e. $0 \leqslant m_1m_2 \leqslant 1$ are predicted and experimentally verified.

The last parameter of Equation 19, the principal relaxation time τ_1, is a complex function dependent on sample polydispersity which can not be readily correlated with a single molecular or rheological function (45). However, the correlation can be obtained through H_G as intermediary.

Using complex algebra principles H_G can be expressed in terms of parameters of either Equation 20 or Equation 21:

$$H_G(\omega) = (2\eta_0/\pi)r_1^{-m_2}\sin m_2\theta_1 = (\eta_0/\pi)r_2^{\beta} \sin \beta\theta_2 \tag{29}$$

where:

$$r_1 \equiv [1+2(\omega\tau_1)^{m_1} \cos(\pi m_1/2) + (\omega\tau_1)^{2m_1}]^{\frac{1}{2}}$$

$$\theta_1 \equiv \arcsin\{(\omega\tau)^{m_1} r_1^{-1} \sin(\pi m_1/2)\}$$

$$r_2 \equiv \{[1-(\omega\tau_2)^{1-\alpha} \sin(\pi\alpha/2)]^2 + (\omega\tau_2)^{2(1-\alpha)} \cos^2(\pi\alpha/2)\}^{\frac{1}{2}}$$

$$\theta_2 \equiv \arctan\{[(\omega\tau^2)^{1-\alpha} \cos(\pi\alpha/2)] / [1-(\omega\tau_2)]^{1-\alpha} \sin(\pi\alpha/2)\}$$

Furthermore, from Equation 21 the real and imaginary parts of η^* can be expressed as:

$$\eta' = (\eta_0/r_2^{\beta}) \cos \beta\theta_2 \tag{30a}$$

$$\eta'' = (\eta_0/r_2^{\beta}) \sin \beta\theta_2 \tag{30b}$$

Comparing Equations 29 and 30 it is evident that for systems whose η^* vs. ω dependence can be described by Equation 21 there is a simple equivalence: $\eta''(\omega) = \pi H_G(\omega)$.

The molecular weight dependence enters Equation 29 through η_0. For this reason it is convenient to define the reduced frequency relaxation spectrum as:

$$\tilde{H}_G(\omega) \equiv H_G(\omega)/\eta_0 \tag{31}$$

An example of this function is presented in Fig. 8. Since the integral:

$$\int_{-\infty}^{+\infty} \tilde{H}_G(s)\, d\ln s \equiv 1 \tag{32}$$

the coordinates of $\tilde{H}_G(\omega)$ maximum (ω_{max}, $\tilde{H}_{G,max}$) should correlate with the molecular parameters of the melt. Indeed, it can be shown that in single phase systems ω_{max} depends on η_0 and $\tilde{H}_{G,max}$ on sample polydispersity (11, 14, 54). These dependencies are presented in Fig. 9. It is evident that for Series I blends there is a linear correlation between log ω_{max} and log η_0 as well as between log $\tilde{H}_{G,max}$ and M_n/M_w but for LLDPE/LDPE, Series II, the linearity is not observed.

The linearity of dependencies in Fig. 9 can be predicted assuming miscibility in a blend composed of polymers with similar molecular weights. For such systems the general, third order mixing rule for relaxation spectrum (55, 56):

$$H(\tau) = \sum_{ijk} P_{ijk} H_{ijk} (\tau/\Lambda_{ijk}) \tag{33}$$

can be reduced to simple additivity:

$$H(\tau) = \sum w_i H_i(\tau) \tag{34}$$

In Equation 33 P_{ijk} is the third order intensity function (replaced in Equation 33 by the weight fraction w_i) and Λ_{ijk} is the third order interactive relaxation time factor, which originates in the intermolecular interactions between dissimilar molecules. In homologous polymer blends where the molecular weight of one polymer is lower than the entanglement molecular weight, M_e, and that of the second is higher than M_e, Equation 34 must be extended to accommodate a second order term (57).

The proposed method of data treatment has two advantages: (i) it allows assessment of the status of blend miscibility in the melt, and (ii) it permits computation of any linear viscoelastic function from a single frequency scan. Once the numerical values of Equation 20 or Equation 21 parameters are established the relaxation spectrum as well as all linear viscoelastic functions of the material are known. Since there is a direct relation between the relaxation and the retardation time spectra, one can compute from $H_G(\omega)$ the stress growth function, creep compliance, complex dynamic compliances, etc. (58). However, one must keep in mind that validity of the computed functions is only assured within the range of independent variables (ω,T,P,t,...) used in determining H_G. For example:

$$G'_{calc}(\omega) = \int_{-\infty}^{+\infty} \{s\, H_G(s)/[1+(s/\omega)^2]\}\, d\ln s \qquad (35a)$$

$$G''_{calc}(\omega) = \int_{-\infty}^{+\infty} \{\omega\, H_G(s)/[1+(\omega/s)^2]\}\, d\ln s \qquad (35b)$$

$$\eta^+_{calc}(t) = \int_{-\infty}^{+\infty} H_G(s)[1-\exp\{st\}]\, d\ln s \qquad (36)$$

where η^+ is the stress growth shear viscosity. In Fig. 10 the experimental values of G' for blends Series I and II (points) are compared with G'_{calc} (lines) computed from H_G which in turn was determined using the η'-data. The agreement is quite satisfactory with residuals $|G' - G_{calc}| < 5\%$ for both series. The concluded immiscibility for LLDPE/LDPE blends of Series II make this observation particularly interesting.

Cole-Cole plot

The η'' vs. η' dependence is often used while discussing the dynamic data of polymer blends. Since for simple liquids the plot has the form of a semi-circular arc, deviation from a semi-circle is sometimes identified with immiscibility. However, as frequently demonstrated for homopolymers (16) and homologous polymer blends (59) the form of the η'' vs. η' plot is determined by the shape of the relaxation spectrum; the molecular polydispersity can modify the Cole-Cole plot as much as the presence of the interphase. As a rule, the presence of (unsubtracted) yield stress appears in the plot as a sudden departure from a semi-circular pattern at higher η' level.

From Equations 29 and 30 it is evident that both $H_G(\omega)$ and the Cole-Cole plot contain the same information; in principle these data treatments are equivalent. The advantage of H_G is the straight-forward interpretation and access to other linear viscoelastic functions. The advantage of the Cole-Cole plot is its simplicity - it can be constructed simply by plotting one experimental function versus another.

In accordance with Equation 30 η' and η'' can be normalized by dividing by η_0, i.e. η'/η_0 and η''/η_0. Such a normalized Cole-Cole plot has frequently been used for polymer blends (60, 61). In Fig.

ll the normalized Cole-Cole plot is shown for blends of Series I and II. The data used for constructing the Figure are the same as those used for computation of $\tilde{\eta}_C$ in Fig. 8.

Cross-point coordinates

The coordinates defined as $G_X = G' = G''$ at $\omega = \omega_X$ were reported (62, 63) to be related to the molecular parameters of melts: $G_X \propto (M_w/M_w)^{\alpha}$ and $\omega_X \propto M_w^{\beta}$ with α and β negative. From Equations 34 and 35 it follows that $G' = G''$ at $\omega = s = 1/\tau$, i.e. when the test frequency equals the inversed relaxation time of the system. Substituting this condition into the relation:

$$G'(\omega) = A\eta_0\omega^2\tau/[1+(\omega\tau)^2] \qquad (37)$$

derived for simple liquids with a single relaxation time by Maxwell (A=1) and by Rouse ($A = 6/\pi^2$), one gets:

$$\eta_{0_m} = 2G_X/A\omega_X \qquad (38)$$

In Fig. 12 η_{0m}, calculated with A = 1, is plotted vs. η_0 for LDPE and LLDPE resins and for their blends. The totally unexpected identity $\eta_{0m} = \eta_0$ for $\eta_0 \leqslant 60$ kPas was obtained. Above this limit the values diverged into $\eta_0 = 7\eta_{0m}$ for $\eta_0 > 200$ kPas, where Equation 38 could be valid if $A \simeq 1/7$. From the general Rouse theory (64) A decreases with an increase of polydispersity of the relaxation times but the influence is not large enough to allow such a low A-value. As will be shown in part 4 the dependence presented in Fig. 12 was duplicated by the results of LLDPE/PP blends indicating a broad applicability of Equation 38 (41, 64).

For LLDPE blends the relations reported by Zeichner et al. (62, 63) were not obeyed. For example the plot of G_X vs. w_2 showed an opposite trend from the predicted negative deviation from the additivity rule.

For LLDPE and their blends the activation energy of flow $E_\sigma \equiv R(\partial \ln \eta/\partial\ 1/T)_\sigma = \text{const} = E_{\dot{\gamma}}^{\cdot}/n = 30 \pm 2$ kJ/mol was found (45).

The uniaxial extensional flow

The behavior of LLDPE blends at constant rate of stretching, $\dot{\varepsilon}$, was examined at 150°C. The results are shown in Fig. 13 for Series I and II as well as in Fig. 14 for Series III. The solid lines in Fig. 13 represent $3\eta^+_{calc}$ values computed from the frequency relaxation spectrum by means of Equation (36), while triangles indicate the measured in steady state $3\eta^+$ values at $\dot{\gamma} = 10^{-2}$ (s^{-1}), i.e. the solid lines and the points represent the predicted and measured linear viscoelastic behavior respectively. The agreement is satisfactory. The broken lines in Fig. 13 represent the experimental values of the stress growth function in uniaxial extension, η_E^+. The distance between the solid and broken lines is a measure of nonlinearity of the system caused by strain hardening, SH.

The SH plays a positive role in film blowing (15, 44) or in wire coating (66). LPX-30 does not show this effect and its on line

processability index is low. On the other hand, SH of LDPE is quite high and so is the processability index. The accepted mechanism for improvement of film bubble stability is self healing of a potentially weak spot by a local increase of extensional viscosity caused by SH. It is important to note that adding to LPX-30 either 10 wt% LDPE, 20% LLDPE-10 or 10% LPX-24 was sufficient for generation of SH. The subsequent trial on a production line confirmed these results; increased bubble stability allowed for higher production rates of the blends.

Figs. 13 and 14 also provide information on sample polydispersity. The initial slope of the stress growth function can be expressed as:

$$S = d\ln \eta_E^+ / d\ln t \Big|_{\text{low } t} \tag{39}$$

For a series of LLDPE's the relation presented in Fig. 15 was found. An explanation for this empirical correlation can be found in Gleissle's mirror image principle (67):

$$\eta(\dot{\gamma}) = \eta^+(t); \quad t \propto 1/\dot{\gamma} \tag{40}$$

Accordingly, S is equivalent to:

$$S = d\ln \eta / d\ln \dot{\gamma} \Big|_{\text{high } \dot{\gamma}} = n-1$$

where n is the power law index. Both (n-1) and S are related to polydispersity (68) Since for miscible blends the polydispersity can be calculated from Equations 15 to 18, the dependence in Fig. 15 provides a means for detecting miscibility in samples under uniaxial extensional flow. The data in Fig. 16 show the experimental S vs. w_2 dependence (points) as well as that predicted from variation of the polydispersity with composition (broken lines) for blends of Series I and II. The data in Fig. 16 confirm the previous results suggesting that while LLDPE/LLDPE Series I blends are miscible, those of LLDPE with LDPE, Series II blends, are not.

The S vs. w_2 dependence for Series III shown in Fig. 17 is particularly interesting. Apparently, upon addition of a small quantity of LPX-24, $w_2 \leqslant 20\%$, the polydispersity increases, as it should for a miscible system. However, for $w_2 > 20\%$ the polydispersity seems to decrease. Phase separation in the vicinity of 20 wt% of LPX-24 could provide a mechanism for such behavior.

Curve No. 1 in Fig. 1 shows the $\eta_E = \eta_E(\dot{\varepsilon} = 0.1\ s^{-1})$ dependence on w_2 for Series III blends. The points are experimental, the curve is a third order polynomial. Similarity of the shape of this dependence and that shown in Fig. 17 allows postulation that both are caused by the phase behavior. It is worth pointing out that the extrema on the η_E vs. w_2 plot represent compositions which may be of particular interest for processors: at the maximum the effect of LPX-24 on the stress hardening is most pronounced and the

composition is most suitable for film blowing. At the minimum the η_E, and parallel with it the shear viscosity, is the lowest. The extrudability of LPX-24 with about 10 to 20 wt% LPX-30 is most efficient and stable. The usefulness of blends with compositions corresponding to extrema in the property-concentration dependence was recognized by Plochocki, who labeled these as the "rheologically particular compositions", or RPC (8). According to that author the shape of a rheological function vs. composition dependence is paralleled by a similar relation between the density and concentration. Judging by information in Fig. 17 it is the phase separation which provides the mechanism responsible for variation of density of Series III blends.

From the dependence: $\eta^+ = \eta^+ (\dot{\varepsilon},t)$ in Fig. 13 the values of the equilibrium extensional viscosity, η_E, were determined and plotted in Fig. 18. Operationally, η_E was taken as the maximum value of η_E at a given $\dot{\varepsilon}$. For specimens with maximum strain at break ε_b larger than the rheometer limit, $\varepsilon_L = 3.2$, the arrow on a side of the data point was placed. The η_E vs. $\dot{\varepsilon}$ dependences for Series I are simple, resembling the classical shear flow curves, η vs. $\dot{\gamma}$. The few arrows indicate that for most of these blends $\varepsilon_b \leqslant 3.2$. By contrast, the plot for Series II is quite complex. Note that for several blends η_E as well as $\varepsilon_E > 3.2$ are larger than those for neat polymers. The complex shape of η_E vs. $\dot{\varepsilon}$ dependence for II.50 blend is particularly noticeable. Apparently the co-continuous blend morphology, expected at this concentration, resulted in self-reinforcing behavior, more sensitive to the rate of deformation than that observed for II.10 (LPX-30 with 10% LDPE) where the dispersed LDPE drops were transformed by uniaxial stress into reinforcing short fibers.

In Fig. 19 the steady state uniaxial elongational viscosity, $\eta_E/3$, is compared with the steady state shear, η, as well as dynamic, η', and complex, η^*, viscosities. It is evident that some strain hardening, evident in I.100 (LLDPE-10) is systematically diluted by the increasing amount of LPX-30. Thus, Series I behaves as a truly miscible system. By contrast, addition of LDPE (II.100) to LPX-30 (I.0) is generating more a complex variation of properties. The strain hardening, already visible at 10% of LDPE, reaches its maximum <u>not</u> at 100% LDPE but rather at 50:50 composition. Note that at $\dot{\varepsilon} \geqslant 0.1$ (s^{-1}) the maximum strain at break for II.50 is $\varepsilon_b > \varepsilon_L = 3.2$. The blends behave as immiscible.

The strain hardening, SH, causes the polymer to show a dual nature; at low strains it behaves as a linear viscoelastic liquid, whereas at high ones the non-linearity suggests a network-like behavior. For this reason the η_E vs. w_2 dependence may be misleading - it is not known where the linear behavior ends and SH begins. This is why in Fig. 20 only the linear viscoelastic part of η_E^+ is shown, the part computed from H_G by means of Equation 36. A significant difference in behavior between Series I and Series II is again visible at all deformation rates. For Series I the values of $3\eta^+_{calc}$ show simple additivity, whereas for Series II, there is a positive deviation from the log-additivity rule, PDB. While the PDB behavior per se is insufficient to call immiscibility,

The rheological testing was carried out in RMS and ICR at 190°C and in RER at 150°C. The instruments and procedures were described in the preceeding part.

Preliminary tests

Both the theoretical and experimental studies indicated that the highest degree of dispersion can be obtained blending two liquids with similar viscosities at the same stress level as that expected during mixing:

$$\lambda_{opt} \equiv \eta_1/\eta_2 = 0.3 \text{ to } 1.0$$

where subscript 1 indicates the dispersed polymer and 2 indicates the matrix (11, 42, 43). For this reason PP-1 and LLDPE-A were chosen as the most suitable pair (39). The samples containing 0, 50 and 100 wt% LLDPE-A were studied. The 50:50 blends containing 0 or 10% EP-1 or EP-2 were labeled: BL, BL-1 and BL-2, respectively.

The capillary flow. The interlayer slip apparent in uncompatibilized blend, BL, disappears upon addition of EP-1 or EP-2. Δ the slip affected the entrance-exit pressure drop, P_e, ("Bagley correction") more than viscosity. In Fig. 21 P_e vs. σ_{12} is shown for blends with and without EP's.

The second interesting observation based on ICR and RMS results is related to the need for pressure correction in capillary flow. Already in Fig. 19 an agreement between the dynamic viscosity, η', and corrected for pressure effect capillary shear viscosity, η, was shown. In Fig. 22 five different measures of viscosity are shown for LLDPE-A (four for the other samples): steady state elongational viscosity, $\eta_E/3$, complex and dynamic viscosity, η^* and η', as well as the steady state capillary viscosity corrected and uncorrected for the pressure effects, η_{corr} and η(ICR) respectively. There is a double equivalence of data points: $\eta_{corr} \approx \eta'$ and $\eta(ICR) \approx \eta^*$. The latter equivalence has a form of an apparent Cox-Mertz rule. Evidently the true steady state viscosity for LLDPE with the narrow molecular weight distribution requires the pressure correction. When the data are properly corrected the equivalence between the steady state shear viscosity and the loss-part of complex viscosity is found. On the other hand, neglecting the pressure corrections results in coincidental equivalence between η(ICR) and η^*.

In agreement with the polydispersity data in Table IV for PP the pressure correction was significantly smaller than that determined for LLDPE-A. For the blends the correction was reduced even further, suggesting that molecular weight distribution in the phase adjacent to the capillary wall is broader than that of either polymeric component, indicating that LLDPE-A and PP may be partially miscible.

The Dynamic flow. The flow curves, η' vs. ω in Fig. 22, were not corrected for the apparent yield stress. For PP and LLDPE-A the curves nearly reached the Newtonian plateau and the Cole-Cole plots were found to be semi-circular indicating that $\sigma_y \approx 0$. However, for blends the situation is less clear. Judging by the flow curves for BL, BL-1 and BL-2 at low deformation rates, the Newtonian plateau

seems to be far away. This may indicate the incipient yield stress. To clarify this point η'' vs. η' was plotted in Fig. 23. An onset of the second relaxation mechanism is visible. The long relaxation times in BL may only originate in the interphase interactions. These usually lead to the presence of the apparent yield stress.

The high frequency cross point coordinates (G_x, ω_x) were used for calculation of the Maxwellian zero-shear viscosity, η_{0M}, from Equation 38. For the neat polymers η_{0M} was in agreement with η_0 calculated from the shear and extensional responses. For BL, BL-1 and especially BL-2 $\eta_{0M} \neq \eta_0$. The presence of an apparent yield stress is the most likely explanation for the discrepancy.

The extensional flow. The stress growth functions in shear (η^+, labelled RMS) and extension, η_E^+, are shown in Fig. 24. The dependencies for all five materials are similar. There is an excellent agreement between η_E^+ and $3\eta^+$. Note the absence of strain hardening, SH, clearly visible (see Figs. 13 and 14) in blends of similar to LLDPE-A polymer, the LPX-30. For PP a strain thinning effect may be suspected. In Fig. 22 the steady state viscosities for PP and BL $\eta_E(\varepsilon) \simeq 3\eta(\omega)$ were reported. For the other samples $\eta_E > 3\eta$ was observed, but the departure from equality was small.

The initial slope S of the relation shown in Fig. 24 was calculated according to Equation 39. For the two homopolymers S increased with M_z/M_n in accord with data presented in Fig. 15. For blends, S was above average indicating partial miscibility.

Summary. The following observations are worth noting: (i) The blends were prepared from relatively low molecular weight, nearly isoviscous polymers. They were immiscible, although the rheological data indicated broadening of the relaxation time spectrum, consistent with partial miscibility of the lowest molecular weight fractions. (ii) The partial miscibility was not sufficient to prevent the interlayer slip in capillary flow; for this purpose a compatibilizing block copolymer had to be added. (iii) The capillary flow data for polymers with narrow molecular weight distribution should be corrected for the pressure effects; after correction the equivalence $\eta \simeq \eta'$ was found. (iv) For the deformation rates ω, $\dot{\gamma} > 10^{-2}$ sec the apparent yield stress is unimportant. (v) There is no strain hardening in extension for PP-1, LLDPE-A and their blends.

PP blends with LLDPE (40, 41, 69)

Polypropylene PP-2 was blended either with LLDPE-B (System-1) or LLDPE-C (System-2). The homopolymer characteristics are given in Table IV. In each system there were seven blends containing 0, 5, 25, 50, 75, 95 and 100 wt% PP.

Neat polymers and their blends were studied in dynamic shear field (using RMS) and in constant shear stress field using Rheometric Stress Rheometer, RSR. The molecular parameters of polymers and blends were determined by Size Exclusion Chromatography in trichlorobenzene at 140°C. The morphology of freeze-fractured specimens was characterized in Scanning Electron Microscope, SEM, Jeol JSM-35CF.

Molecular weights. The number, weight and average molecular weights, M_n, M_w and M_z, respectively are shown in Fig. 25. The broken lines represent the dependencies predicted by Equations 15 to 17. There is good agreement between the experiment and predictions for samples continuing less than 75% PP; for PP-rich samples the experimental data indicate degradation. It is worth pointing out that within the experimental error the molecular weights of neat PP before and after compounding/extrusion were the same (indicated by a bar in Fig. 25). Thus PP degrades only in the presence of LLDPE. The extent of this effect is larger for higher molecular weight LLDPE-B than LLDPE-C. It primarily affects the highest molecular weight fractions, reducing M_w and M_z but leaving M_n virtually unaffected. The responsible mechanism seems to be shear degradation of PP catalyzed by LLDPE or rather by same its impurities.

Morphology. The SEM of freeze-fractured System-1 specimens indicates dispersed droplet morphology in blends containing 5, 75 and 95% PP and co-continuous structure for the remaining blends containing 25 and 50% PP. In System-2 co-continuous morphology for 50% PP blends was observed.

The apparent yield stress. The complex viscosity η^* vs. ω for PP blends with LLDPE-B and LLDPE-C is shown in Fig. 26. The plot clearly indicates possible yield stress behavior especially for blends containing 50% PP. The apparent yield stress in dynamic flow data was calculated using Equation 22, with $F = G'$ or $F = G''$. The yield stress values as well as the assumed matrix material for calculating F_m are listed in Table V. For both systems the maximum value of the apparent yield stress occurred at 50% PP. In fact, there is a direct correlation - in a given system the yielding is primarily observed in blends having a co-continuous structure. As before (53) $G'_y > G''_y$.

In the last column of Table V the directly measured shear stress values at yield are listed. These measurements were carried out in RSR, setting the desired level of stress and recording the strain after 200 s. The results are shown in Fig. 27. There is good agreement between G'_y and σ_y for System-1 but not for System-2. The two sets of experiments are carried out on a different time scale. Since, according to Equation 24,the apparent yield stress in blends depends on time one should not expect the same results from the dynamic and creep measurements. The differences in less viscous system-2 are expected to be larger than those for System-1.

The frequency dependence of data [corrected for the yield stress by means of Equation 25] was found to follow Equation 19. Having established values of the four parameters: η_0 τ_1, m_1 and m_2 the relaxation spectra were computed from Equation 29. These are shown in Fig. 28. For verification of the procedure $G'_{calc}(\omega)$ was computed from Equation 35. In Fig. 29 its values are compared with experimental $G'(\omega)$ data uncorrected for the yield stress. Furthermore, knowing η', the loss modulus, G''_{calc}, as well as the yield values for G' and G" it was possible to compute $\eta^* = \eta^*(\omega)$ dependence. These values are shown as lines intersecting the experimental data points in Fig. 26.

The concentration dependence of η_0 computed from Equation 20 is shown in Fig. 30, where the solid points represent the experimental data and the open points their values corrected for the effects of PP degradation. For System-1 there is strong negative deviation (NDB) from the log additivity rule, viz. Equation 1, but for System-2 NDB is visible at low PP content, converting to positive deviation (PDB) at high. It is worth recalling that η_0 was computed from corrected for the yield stress values of η'. The NDB behavior, indicative of interlayer slip, reflects poor miscibility in System-1 and that at low concentration of PP in System-2. The emulsion-like behavior of System-2 at high PP content reflects a better interphase interaction.

The Cole-Cole plot for System-2 is presented in Fig. 31. A "classical" semi-circular dependence was obtained for blends containing 0, 5, 25, 95 and 100% PP. For the remaining two blends with 50 to 75% PP there is an indication of a bimodal relaxation spectrum. For this system the bimodality cannot be generated applying a mixing rule to the homopolymer spectra. Clearly an influence of the interphase is responsible for the apparent yield stress. The dependence for System-1 shows a departure from semi-circular behavior for blends containing 5, 25 and 50% PP but none for those with 0, 75, 95 and 100% PP.

If the appearance of bimodality of the relaxations in Cole-Cole plot is equated with formation of co-continuous structure, then in System-1 these occur at 5 to 40 wt% PP whereas in System-2 at 50 and 75 wt% PP. Paul and Barlow proposed the following dependence (70):

$$\phi_i/(1-\phi_i) = \eta_1/\eta_2 \qquad (42)$$

where ϕ_i is the volume fraction of the dispersed phase inverting into the continuous and η_1, η_2 are viscosities of the dispersed and continuous phases. Assuming that the shear stress in the compounding extruder was about 10 kPa, then Equation 42 predicts inversion at 8 to 79% of PP in System-1 and -2, respectively. The direct SEM observations indicate dispersed structures at 5% but co-continuous ones at 25 and 50% PP in System-1 as well as at 50 and 75% PP in System-2. It is apparent that phase inversion, takes place via co-continuous structure. Equation 42 seems to predict the inversion concentration fairly well. However, the co-continuous structure is observed not only near the predicted ϕ_i but also at 50:50 loading where the volume fractions of the two polymers are nearly equal. The broadening of the inversion region from a single ϕ_i to a wide range of composition including equi-volumetric most likely is due to a non-equilibrium nature of morphology.

The cross-point coordinates $G_x \equiv G' = G''$ at $\omega = \omega_x$ were determined for all compositions then the Maxwellian viscosity η_{0M} was calculated from Equation 38. The results are shown in Fig. 32 as η_{0M} vs. η_0. In agreement with the previously discussed data for LLDPE blends (see Fig. 12) initially $\eta_0 = \eta_{0M}$; only for higher values: $\eta_0 > 100$ kPas, there is a deviation from equality.

Summary

The PP/LLDPE blends are immiscible and the degree of incompatibility increases with molecular weight of the homopolymers. An increase of molecular weight shifts the appearance of the apparent yield stress to higher frequencies accessible in standard test equipment. The yield stress seems to be associated with flow and deformability of co-continuous blend structure. The co-continuous morphology stretched from the concentration predicted by Paul and Barlow's empirical equation up to equi-volume polymer concentration. The flow curves, corrected for the yield stress, could be described by the four-parameter equation, which in turn lead to the spectrum of relaxation times and derivation of other linear viscoelastic functions in good agreement with directly measured values.

There are several other observations important for those interested in PP/LLDPE rheology, but their generality is uncertain. An example of these is the strain softening for PP or LLDPE-induced degradation of PP. The information is complex but self-evident. Working for years with these "simple" polymers one is continuously surprised how diverse their behavior can be.

CONCLUSIONS

The similarities and differences between LLDPE blends with LLDPE, LDPE and PP are summarized in Table VI.

NOTATION

a	= coefficient in Equation 23
a_i, b_i	= coefficients in Equations 11 and 12
B	= extrudate swell
C_i	= polynomial coefficients in Equation 8
C_n	= n-paraffins
d	= capillary diameter
D	= extrudate diameter
EPR, EPDM	= binary and ternary copolymers of ethylene and propylene
E_σ, $E_{\dot{\gamma}}$	= activation energy of flow at constant stress or rate of shear
F, F_a, F_y, F_m	= rheological function, its apparent, yield and in the matrix value
F_y^∞	= high frequency yield stress

G', G'', G^*	= storage, loss and complex shear modulus (Pa)
$G_x \equiv G' = G''$	= cross-point shear modulus (Pa)
HDPE	= high density PE
H_G, $\tilde{H}_G$	= frequency relaxation spectrum and H_G/η_0
$\tilde{H}_{G,max}$	= maximum value of $\tilde{H}_G$
i	= $\sqrt{-1}$
Im	= imaginary part of a complex function
J_e	= steady state compliance
L	= capillary length
LCB	= long chain branching
LDPE	= low density polyethylene
LLDPE	= linear LDPE
L_0, L_∞	= specimen length at $t = 0$ and $t = \infty$
m_i	= parameters of Equation 20
M_n, M_w, M_z, M_η	= number, weight, z- and η-average MW
MW	= molecular weight
MWD	= molecular weight distribution
n	= power-law exponent
N_1	= first normal stress difference
NDB	= negative deviating blends
P	= total pressure loss in capillary flow (Pa)
PDB, PNDB	= positive, positive-negative deviating blends
P*	= pressure reducing factor
P_e	= capillary end effects pressure loss (Pa)
PE	= polyethylene
PP	= polypropylene

Q	= extruder output
r^2	= correlation coefficient squared
r_i	= function defined in Equation 29
Re	= real part of a complex function
R_T, $R_{T,0}$	= Trouton ratio at finite and zero rate of deformation, respectively
s	= variable
S	= initial slope defined in Equation 39
SCB	= short chain branching
SEC	= size exclusion chromatography
SH	= strain hardening
t	= time
T	= temperature (°C)
T^*	= temperature reducing factor
ULDPE	= ultra low density PE
VLDPE	= very low density PE
w_i	= weight fraction of polymer
α, β	= parameters
β_1, β_{12}	= slip coefficient and its intrinsic value
γ	= shear strain in dynamic tests
$\dot{\gamma}$	= shear rate (1/s)
ε, ε_b	= Hencky strain, strain at break
$\dot{\varepsilon}$	= strain rate in extension (1/s)
η	= steady state shear viscosity (Pa•s)
η'	= dynamic shear viscosity
η_0, η_{0_M}	= zero-shear viscosity and η_0 for Maxewellian liquid
η^+_{calc}	= compted from H_G stress growth function in shear

η_E, $\eta_{E,0}$	= uniaxial extensional viscosity at finite and zero deformation rate (Pa·s)
$\eta^+_{E,lin}$	= linear viscoelastic component of the stress growth function in uniaxial tension
η^+_E, η^+	= stress growth function in uniaxial extension and shear
η^*	= complex viscosity
λ	= viscosity ratio
θ	= function defined by Equation 29
ϕ_i	= volume fraction
ρ	= density (kg/m^3)
σ_b	= extensional stress at break (Pa)
σ_{11}	= extensional stress (Pa)
σ_{12}	= shear stress (Pa)
τ_i	= primary relaxation time (s)
τ_y	= relaxation time of a network
ω	= angular frequency (rad/s)
ω_x	= cross-point frequency
ω_{max}	= frequency for maximum of $\tilde{H}_G$

LITERATURE CITED

1. Anon., Chem. Market. Reporter 1987, pg 3, 23.
2. Ruof, M.; Fritz, H.-G.; Geiger, K. Kunststoffe, 1987, 77, 480.
3. Romanini, D. Polym.-Plast. Technol. Eng. 1982, 19, 201.
4. Nowlin, T.E. Prog. Polym. Sci. 1985, 11, 29.
5. Keii, T.; Soga, K., Eds. Catalytic Polymerization of Olefins, Kodansha, Tokyo, 1986.
6. "Modern Plastics Encyclopaedia - 1988", McGraw-Hill, New York, 1987.
7. Plochocki, A.P. Trans. Soc. Rheology 1976, 20, 287.
8. Plochocki, A.P. In Polymer Blends; Paul, D.R; Newman, S., Eds.; Academic Press, New York, 1978.
9. Plochocki, A.P. Polym. Eng. Sci. 1982, 22, 1153.

10. Utracki, L.A. Adv. Plast. Technol. 1985, 5, 41: J. Elastom. Plast. 1986, 18, 177.
11. Utracki, L.A. Industrial Polymer Blends; Hanser V., München, 1989.
12. Dobrescu, V. In Rheology; Astarita, G.; Marrucci, G. and Nicolais, L., Plenum Press, New York, 1980.
13. Chuang, H.-K.; Han, C.D. J. Appl. Polym. Sci. 1984, 29, 2205.
14. Utracki, L.A.; Schlund, B. Polym. Eng. Sci. 1987, 27, 1512.
15. Schlund, B.; Utracki, L.A. Polym. Eng. Sci. 1987, 27, 1523.
16. Dumoulin, M.M.; Utracki, L.A.; Lara, J. Polym. Eng. Sci 1984, 24, 117.
17. Vadhar, P.; Kyu, T. Polym. Eng. Sci. 1987, 27, 202.
18. Stehling, F.C.; Wignall, G.D. A.C.S. Polym. Prepr. 1983, 24, 211.
19. Bates, F.S.; Wignall, G.D. Macromolecules 1986, 19, 932, 1938.
20. Ree, M.; Kyu, T.; Stein, R.S. J. Polym. Sci., B. Polym. Phys. 1987, 25, 105.
21. Kammer, H.W.; Socher, M. Acta Polym. 1982, 33, 658.
22. Curto, D.; La Mantia, F.P.; Acierno, D. Rheol. Acta. 1983, 22, 197.
23. La Mantia, F.P.; Curto, D.; Acierno, D. Acta. Polym. 1984, 35, 71.
24. Santamaria, A.; White,J.L. J. Appl. Polym. Sci. 1986, 31, 209.
25. Speed, C.S. Plast. Eng. 1982, 38, 39.
26. Nancekivell, J. Canad. Plast. 1985, 43(1), 28; 1985, 43(9), 27.
27. Acierno, D.; Curto, D.; La Mantia, F.P.; Valenza, A. Polym. Eng. Sci. 1986, 26, 28.
28. La Mantia, F.P.; Valenza, A.; Acierno, D. Polym. Bull., 1986, 15, 381.
29. Ghijsels, A.; Ente, J.J.S.M; Raadsen, J. Rolduc Meeting 2, 1987.
30. Deanin, R.D; D'Isidoro, G.E. A.C.S. Org. Coat. Plast. Div. Preprints 1980, 43, 19.
31. Bartlett, D.W.; Barlow, J.W; Paul, D.R. J. Appl. Polym. Sci. 1982, 27, 2351.
32. Alle, N.; Lyngaae-Jorgensen, J. Rheol. Acta. 1980, 19, 94, 104.
33. Alle, N.; Andersen, F.E; Lyngaae-Jorgensen, J. Rheol. Acta. 1981, 20, 222.
34. Lin, C.-C. Polym. J. 1979, 11, 185.
35. Valenza, A.; La Mantia, F.P.; Acierno, D. Eur. Polym. J. 1984, 20, 727.
36. Kubicka, H; Wozniak, T. Prace Inst. Wlokiennictwa (Lodz) 1977, 27, 57.
37. Plochocki, A.P. Adv. Polym. Technol. 1983, 3, 405.
38. Santamaria, A.; Munoz, M.E.; Pena, J.J.; Remiro, P. Angew. Makromol. Chem. 1985, 134, 63.
39. Dumoulin, M.M.; Farha, C.; Utracki, L.A. Polym. Eng. Sci. 1984, 24, 1319.
40. Dumoulin, M.M. PhD thesis, Ecole Polytechnique, Montreal, Canada, 1988.

41. Dumoulin, M.M.; Utracki, L.A. CRG/MSD Symposium, Hamilton Ont., June, 1984.
42. Utracki, L.A. In Current Topics in Polymer Science; Ottenbrite, R.M.; Utracki, L.A.; Inoue, S., Eds., Hanser V., München, 1987.
43. Utracki, L.A. In Rheological Measurements; Collyer, A.A.; Clegg, D.W., Eds.; Elsevier Appl. Sci. Publ., London, 1988.
44. Schlund, B; Utracki, L.A. Polym. Eng. Sci. 1987, 27 359, 380.
45. Utracki, L.A.; Schlund, B. Polym. Eng. Sci. 1987, 27 367.
46. Utracki, L.A.; Sammut, P. unpublished.
47. Utracki, L.A. Effect of Polydispersity on the Pressure Gradient of Shear Viscosity, 36th Canadian Chem. Eng. Conf., Sarnia, Ont., Canada Oct. 5-8, 1986.
48. Simha, R.; Somcynsky, T. Macromolecules 1969, 2, 342.
49. Tremblay, B.; Utracki, L.A. 4th Annual Polymer Processing Society meeting, Orlando FA, May 8-11, 1988.
50. Havriliak, S.; Nagami, S. Polymer 1967, 8, 161.
51. Utracki, L.A. Proceed. IUPAC 28th Macromol. Symp., Amherst MA, July 12-16, 1982.
52. Utracki, L.A. S.P.E. ANTEC Tech. Papers 1988, 34, 1192; Polym. Eng. Sci. 1989, 29, 0000.
53. Utracki, L.A.; Sammut, P. NRCC/IMRI Symposium "Polyblends-'88", Boucherville, Que. Canada, Apr. 5 and 6, 1988; Polym. Eng. Sci., 1989, 29, 0000.
54. Utracki, L.A. Proceeding CSChE 37th Conference, Montreal, Que. Canada, 18-22 May 1987.
55. Watanabe, H.; Sakamoto, T.; Kotaka, T. Macromolecules 1985, 18, 1008.
56. Watanabe, H.; Kotaka, T. Macromolecules 1987, 20, 530, 535.
57. Rubinstein, M.; Helfand, E.; Pearson, D.S. Macromolecules 1987, 20,822.
58. Ferry, J.D. Viscoelastic Properties of Polymers, third edition, J. Wiley & Sons, New York, 1980.
59. Marin, G. PhD Thesis, Université de Pau, France, 1977.
60. Diogo, A.C.; Marin, G.; Monge, Ph. J. Non-Newtonian Fluid Mech. 1987, 23, 435.
61. Ajji, A.; Choplin, L.; Prud'homme, R.E. NRCC/IMRI Symposium "Polyblends - '88", Boucherville, Que. Canada, Apr. 5 and 6, 1988: J. Polym. Sci., Polym. Phys. Ed., in press.
62. Zeichner, G.R.; Patel, P.D. 2nd World Congress Chem. Eng. Montreal, Canada, Oct. 1981; Proceed. 1981, 6, 333.
63. Zeichner, G.R.; Macosko, C.W. Proceed. IUPAC Macromolecular Symposium, Oxford, UK, 1982, P. 861; SPE ANTEC Tech. Papers 1982, 28, 79.
64. Rouse, P.E. Jr. J. Chem. Phys. 1953, 21, 1272.
65. Dumoulin, M.M.; Utracki, L.A.; Carreau, P.J. 36-th Canadian Chem. Eng. Conference, Sarnia, Ont. Canada, Oct. 1986.
66. Utracki, L.A.; Kamal, M.R.; Al-Bastaki, N.M. SPE ANTEC Tech. Papers 1984, 30, 417.
67. Gleissle, W. In Rheology, G. Astarita, Marruci, G.; Nicolais, L., Eds.; Plenum Press, New York, 2, 457, 1980.
68. Graessley, W.W. Adv. Polym. Sci. 1974, 16, 1.

69. Dumoulin, M.M; Utracki L.A. and Carreau, P.J. Rheol. Acta Suppl. 1988, 26, 215; In "Two Phase Polymeric Systems", L.A. Utracki, Ed., Hanser V., München, 1989.
70. Paul, D.R. and Barlow J.W. J. Macromol. Sci., Rev. 1980, C18, 109.

FIGURES CAPTIONS

Fig. 1. Compositional dependence of the zero-shear viscosity for blends of a linear low density polyethylene (LLDPE) with: (1) and (2) different LLDPE resins, and (3) with low density polyethylene, LDPE.

Fig. 2. Extrudate shrinkage (in Hencky strain units) vs. composition of polypropylene/low density polyethylene blends (38).

Fig. 3. The temperature and pressure sensitivity coefficient for LLDPE I blended with either LLDPE 2 (triangles) or LDPE (circles). The broken line is theoretical, computed from variation of polydispersity in (assumed) miscible blends.

Fig. 4. Extrudate swell at 190°C versus weight fraction of the second component in Series-I and II.

Fig. 5. Flow pattern at the entrance to capillary for linear low density/low density polyethlene blend (LLDPE/LDPE) at 190°C and $\dot{\gamma} = 125\ (s^{-1})$. From the left hand side: 0,20,50 and 100% of LDPE (49).

Fig. 6. Frequency dependence of dynamic viscosity at 150°C for Series-I (left) and Series-II (right). Points - experimental, lines-computed.

Fig. 7. Molecular weight dependence of the zero-shear viscosity for Series-I and II. The line represents the dependence for neat LLDPE resins (45).

Fig. 8. Reduced frequency relaxation spectrum for Series-I and II. The arrows indicate computed coordinates of the maximum ($\tilde{H}_G$ max ω_{max}).

Fig. 9. a) Correlation between the abscissas of relaxation spectrum maximum and the zero-shear viscosity for Series-I and II; b) Correlation between the ordinate of relaxation spectrum maximum and the polydispersity factor M_n/M_w.

Fig. 10. Storage modulus vs. frequency for Series I LLDPE/LLDPE (left) and for Series-II LLDPE/LDPE blends (right) at 190°C. Points - experimental, solid lines computed from $H_G(\omega)$, broken lines connect the constant - ω data points. Concentration of the second component is given in wt%. The results for each blend is displaced horizontally by one decade.

Fig. 11. Cole-Cole plot for miscible (Series-I) and immiscible (Series-II) polyethylene blends.

Fig. 12. Maxwellian zero-shear viscosity computed from cross-point coordinaters versus η_0 for Series-I and II as well as for neat LLDPE resins.

Fig. 13. Stress growth function for blends of linear low density polyethlene, LLDPE, with (A) another type of LLDPE (miscible, Series-I) and (B) with low density polyethylene (immiscible, Series II). The broken lines represent experimental data in elongation, the triangles indicate experimental data in steady state shearing at $\dot{\gamma}$ = $0.01s^{-1}$. The solid lines were computed from the relaxation spectrum (14).

Fig. 14. Stress growth function in uniaxial extension vs. time for LPX-30/LPX-24 blends (Series-III) at T=150°C and $\dot{\varepsilon}$ = 0.001,0.01, 0.1 and 1 (s^{-1}).

Fig. 15. Initial slopes of the stress growth functions of LLDPE's (containing butene, hexene or octene comonomer) as function of resin polydispersity.

Fig. 16. Compositional dependence of the initial slope of the elongational stress growth function for LPX-30/LLDPE 10 (top) and LPX-30/LDPE (bottom). The broken lines were computed assuming miscibility.

Fig. 17. Initial slope of the stress growth function for LPX-30/ LPX-24 blends vs. composition.

Fig. 18. The elongational viscosity in steady state flow at T = 150°C vs. strain rate for Series-I LPX-30/LLDPE-10 blends (top) and Series-II, LLDPE/LDPE blends (bottom). The data points marked with arrow on a side indicate that equilibrium value has not been reached.

Fig. 19. Comparison of rate of deformation dependence of the steady state (capillary) viscosity, η, (points) with the complex, η^*, (solid line) dynamic, η', (broken line) and extensional viscosity, $\eta_E/3$ (open circles). The data are reduced to common temperature 150°C. Left, Series-I, LLDPE/LLDPE, right Series-II LLDPE/LDPE blends. For clarity, the data of each blend is vertically displaced by one decade.

Fig. 20. Compositional dependence of $3\eta^+_{calc} \approx \eta^+_{E,lin}$ at t = 10 and 100(s) for Series-I (top) and Series-II (bottom).

Fig. 21. Bagley pressure correction term, Pe, versus shear stress, σ_{12}, for BL, BL-1, and BL-2. Data for BL-1 and BL-2 have been displaced horizontally by a factor of 5 and 10 respectively.

Fig. 22. Elongational, η_E, complex, η^*, dynamic, η', and shear, η, viscosities versus strain rate, $\dot{\varepsilon}$, frequency, ω, or shear rate, $\dot{\gamma}$, for (from the top): LLDPE, BL, BL-1, BL-2 and PP at 190°C. The data corrected for pressure effects are shown as full squares. For clarity the traces are displaced vertically each by one decade.

Fig. 23. Imaginary part, η'', versus real part, η', of the complex viscosity for BL, BL-1, and BL-2.

Fig. 24. Comparison of shear, $3\eta^+$, and elongational, η_E^+ time dependent viscosities for PP, BL-2, BL-1, and LLDPE at 190°C.

Fig. 25. Compositional variation of average molecular weights for System 1 (left) and 2. Points - experimental, broken lines - calculated.

Fig. 26. Complex viscosity vs. frequency, η^* vs. ω, for System 1 (top) and 2. Points are experimental, lines computed from the relaxation spectrum.

Fig. 27. Shear strain, γ, as a function of shear stress, σ_{12}, for blends containing 50% of each polymer. Curve 1: PP/LLDPE-1, curve 2: PP/LLDPE-2

Fig. 28. Reduced frequency relaxation spectrum for System 1 (top) and System 2.

Fig. 29. Storage shear modulus vs. frequency, G' vs. ω, for System 1. The points are experimental, uncorrected for the apparent yield stress, the lines computed from the relaxation spectrum.

Fig. 30. Zero shear viscosity, η_0, vs. PP content in Systems 1 and 2.

Fig. 31. Cole-Cole plot, η'' vs. η', for System 2.

Fig. 32. Maxwellian viscosity vs. zero-shear viscosity for Systems 1 and 2.

Table I. Global Consumption of Polyethylene (PE) [1]

No.	Type	Code	Process	Density[(a)]	Consumption[(b)]	
					1986	1990
1.	High density PE	HDPE	low pressure: gas phase, solution or suspension	940-970	8.95	9.96
2.	Linear low density PE	LLDPE	low pressure: gas phase, solution or suspension	915-940	3.4	7.5
3.	Low density PE	LDPE	high pressure pipe or autoclave reactor	915-930	12.3	10.0
4.	Very low density PE	VLDPE	low pressure gas phase or solution process	900-915	0.03	0.2
5.	Ultra low density PE	ULDPE	low pressure gas phase or solution process	~885	?	?

Note: (a) in kg/m^3; (b) in million tons per annum.

Table II. Characteristic parameters of neat PE resins [44 to 46]

No.	Parameter (units)	LPX-30	LLDPE-10	LDPE	LPX-24	
1.	Density (kg/m^3)	918	955	922.5		951
2.	Melt index (190°C, 2.16 kg, g/10 min)	1.0	0.3	6.5		0.3
3.	Molecular weights (kg/mol) M_n	41 ± 2	17 ± 1	16 ± 1		28 ± 1
	M_z	272 ± 27	593 ± 11	225 ± 8		719 ± 30
4.	Polydispersity index (-) M_w/M_n	3.4 ± 0.2	11 ± 2	4.1 ± 0.1	7.6 ± 0.2	
5.	Comonomer concentration (wt%)	C_4/7.4	C_6/1.1	-		C_4/4.5
6.	Catalyst based on	Ti	V	-		Ti
7.	Branches $C_n \leq 10$ per 1000 C atoms	0	0	1.2		0
8.	Zero-shear viscosity η_0 (190°C, kPas)	34	645	9.3		8120

Table III. Composition and Molecular Weights (in kg/mol) of LLDPE Blends.

Code	Polymer Content (wt%)				M_n	M_w	M_z
	LPX-30	LLDPE-10	LDPE	LPX-24			
I. 0	100	0	0	0	41	133	272
I. 10	90	10	0	0	33	114	275
I. 20	80	20	0	0	36	144	357
I. 50	50	50	0	0	25	123	397
I. 80	20	80	0	0	25	151	525
I.100	0	100	0	0	17	152	593
II.0 = I.0	100	0	0	0	41	133	272
II.10	90	0	10	0	36	112	252
II.20	80	0	20	0	34	114	254
II.50	50	0	50	0	29	107	242
II.80	20	0	80	0	19	66	248
II.100	0	0	100	0	16	64	225
III.0 = I.0	100	0	0	0	41	133	272
III.10	90	0	0	10	39	141	340
III.20	80	0	0	20	38	150	401
III.50	50	0	0	50	34	174	548
III.80	20	0	0	80	30	199	659
III.100	0	0	0	100	28	216	719

Table IV. Characteristic parameters of PP/PE neat resins

No.	Parameter	PP-1	PP-2	LLDPE-A	LLDPE-B	LLDPE-C	EP-1/EP-2[(a)]
1.	Manufacturer	Hercules	Hercules	Esso	Exxon	Dow Chem.	Hercules
2.	Designation	6704	6701	LLDPE-1	LPX-24	Dowlex 2517	--
3.	Density (kg/m^3)	904	900	918	951	917	901/897
4.	Melt index (g/10 min)	4.0	0.8	1.0	0.3	25	5/0.5
5.	Molecular weights M_n	250	106	97.5	28.4	36	-
	(kg/mol) M_w	325	392	261	216	108	-
6.	Zero shear viscosity, 190°C, η_0 (k Pas)	8.5	13	13	8120	1.32	5.2/6.3

Note: (a) Ethylene - propylene - ethylene copolymers with 11 and 14% of ethylene, respectively

Table V. Apparent yield stress for PP blended with LLDPE-B or LLDPE-C

No.	Blend	PP (wt%)	Material	G'_y (Pa)	G''_y (Pa)	σ_y (Pa)
1.	System-1	5	PE	0	0	-
2.		25	PE	40	0	-
3.		50	PP	58	1.0	36
4.		75	PP	0.8	0	-
5.		95	PP	0	0	-
6.	System-2	5	PE	0	0	-
7.		25	PE	0.5	0.2	-
8.		50	PP	5	0	52
9.		75	PP	2	1.4	-
10.		95	PP	0	0	-

Table VI. Summary of rheological beavior of LLDPE-X blends with LLDPE-Y, LDPE and PP

No.	PROPERTY	LLDPE-Y	LDPE	PP
1.	Miscibility with LLDPE-X in the melt	depends on LLDPE-Y type	immiscible	Miscible
2.	Need for pressure correction in capillary flow	Yes	depends on polydispersity	
3.	η (capillary) = η'	Yes	Yes	Yes
4.	Extrudate swell	depends on LLDPE-Y type	large	large
5.	Interlayer slip	No	No	Yes
6.	Presence of apparent yield stress, σ_y	No	Yes	Yes
7.	Frequency dependence	After correcting for σ_y it can be described by a four-parameter equation, then frequency relaxation spectrum and linear viscoelastic functions can be calculated		
8.	Concentration dependence of η_0	depending on type of LLDPE-Y: additive or sigmoidal	goes through a maximum	Sigmoidal or goes through a minimum
9.	Cole-Cole plot	depends on LLDPE-Y type	bimodal	Semicircular for low MW; then bimodal
10.	Cross-point coordinates	$\eta_0 = \eta_{0_M}$ for $\eta_0 < 100$ kPas; above this limit $\eta_0 > \eta_{0_M}$		
11.	Strain hardening in extensional flow	present	strong	absent
12.	Initial slope of η_E^+, S	the value depends on polydispersity		

Table VI. Summary of rheological beavior of LLDPE-X blends with LLDPE-Y, LDPE and PP (cont.)

No.	PROPERTY	LLDPE-Y	LDPE	PP
13.	Maximum strain at break, ε_b	$\leqslant 3.2$	> 3.2	3.2 depending on $\dot{\varepsilon}$ and concentration
14.	The ratio $\eta_E(\dot{\varepsilon})/3\eta(\omega)$ at $\dot{\varepsilon} = \omega$	> 1	$\gg 1$	≈ 1
15.	Shear degradation	yes	no	yes of PP
16.	The activation energy of flow η (kJ/mole) at constant stress	30 ± 2		

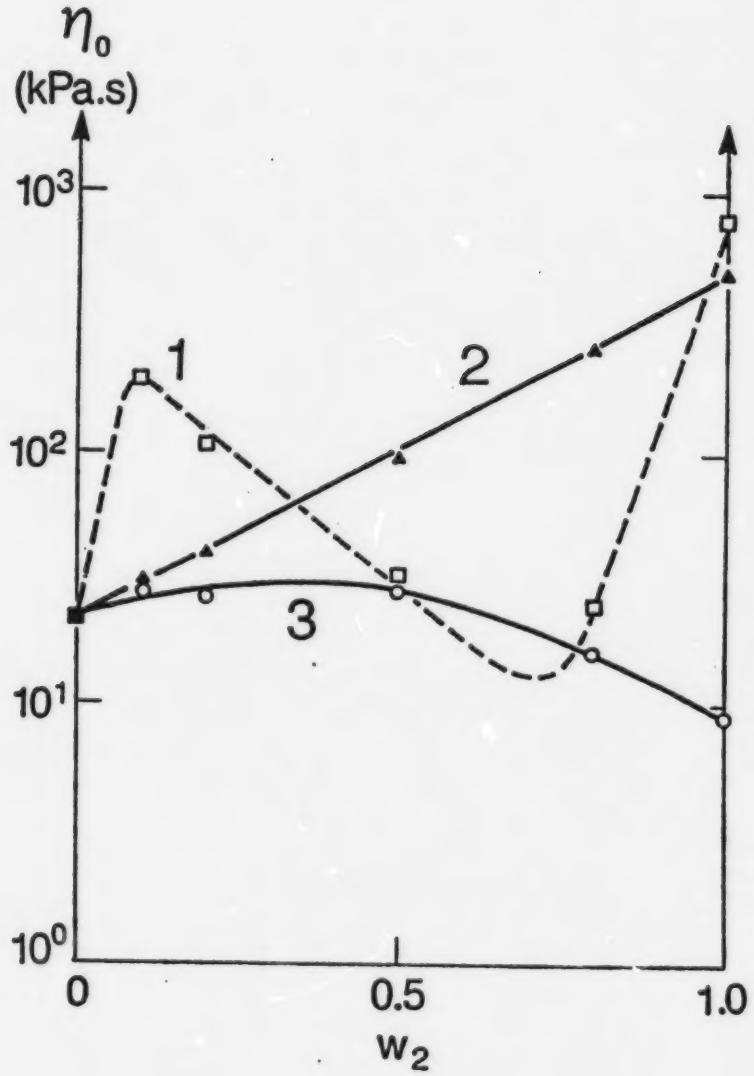

Fig. 1. Compositional dependence of the zero-shear viscosity for blends of a linear low density polyethylene (LLDPE) with: (1) and (2) different LLDPE resins, and (3) with low density polyethylene, LDPE.

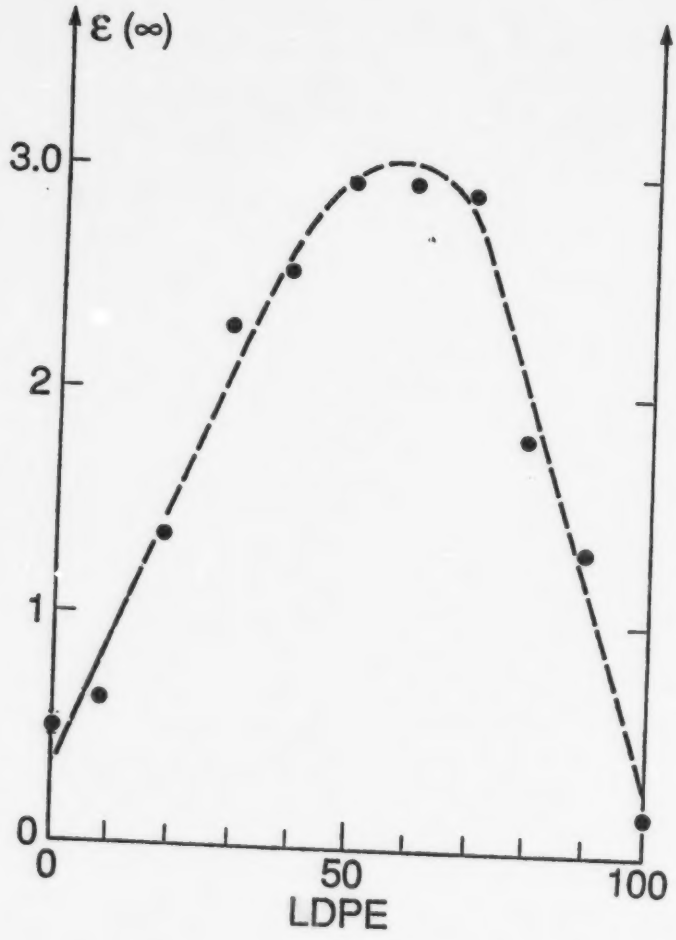

Fig. 2. Extrudate shrinkage (in Hencky strain units) vs. composition of polypropylene/low density polyethylene blends (38).

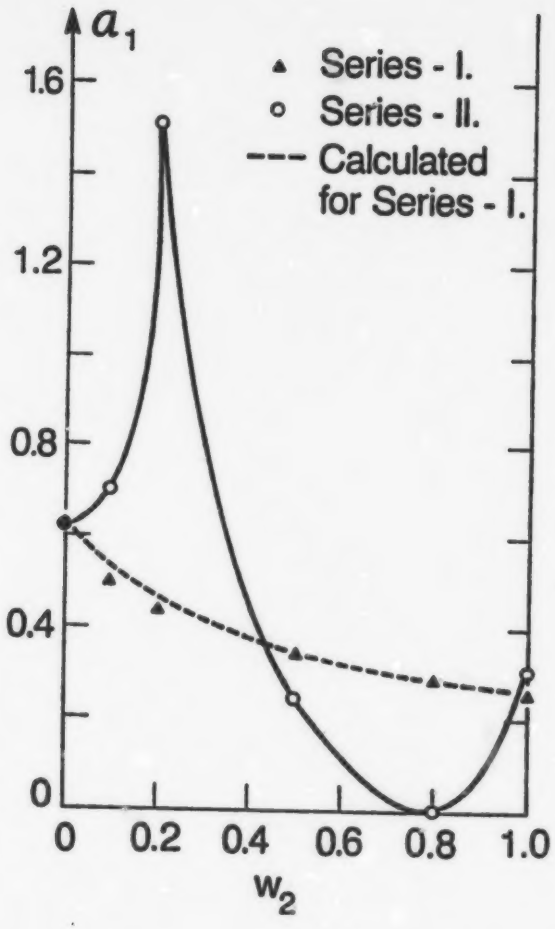

Fig. 3. The temperature and pressure sensitivity coefficient for LLDPE I blended with either LLDPE 2 (triangles) or LDPE (circles). The broken line is theoretical, computed from variation of polydispersity in (assumed) miscible blends.

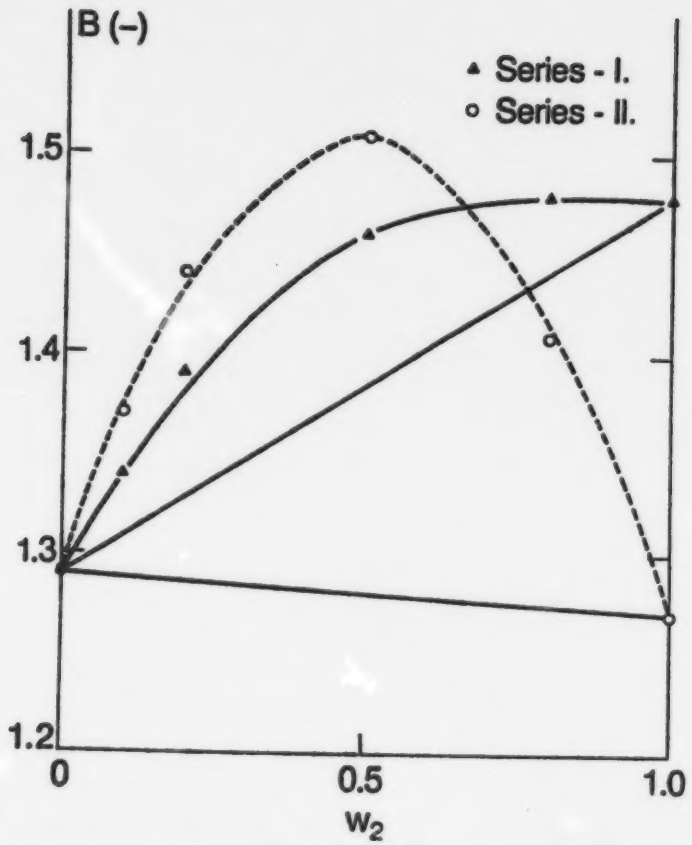

Fig. 4. Extrudate swell at 190°C versus weight fraction of the second component in Series-I and II.

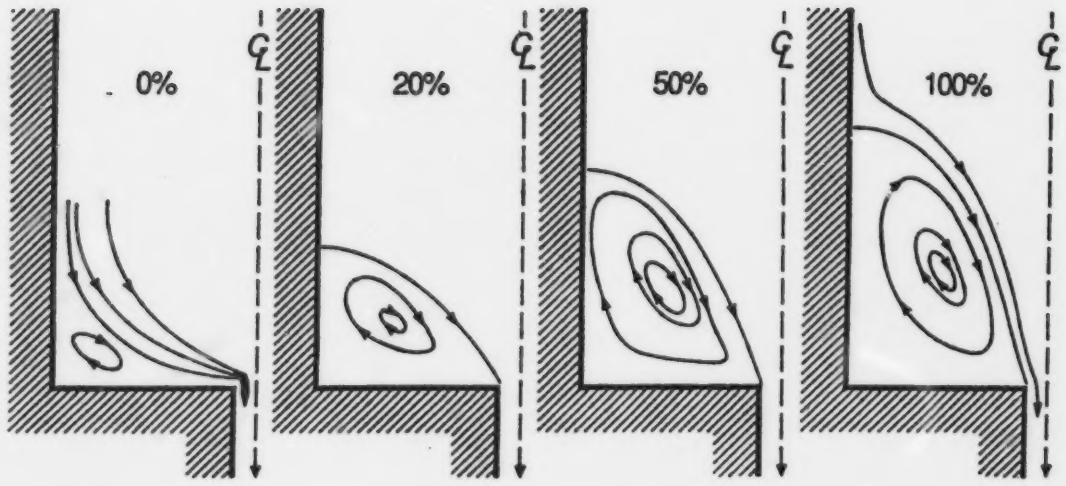

Fig. 5. Flow pattern at the entrance to capillary for linear low density/low density polyethlene blend (LLDPE/LDPE) at 190°C and $\dot{\gamma}$ = 125 (s^{-1}). From the left hand side: 0,20,50 and 100% of LDPE (49).

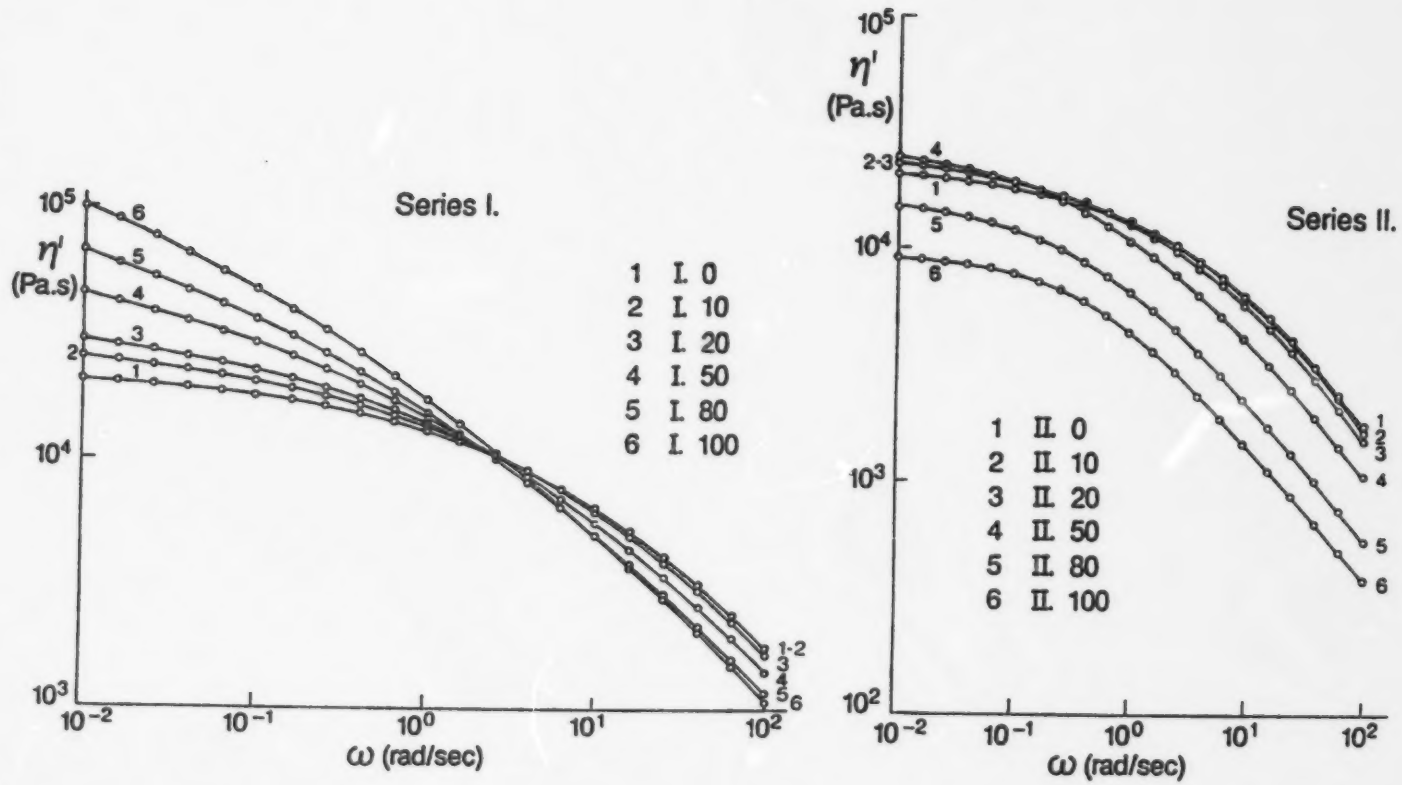

Fig. 6. Frequency dependence of dynamic viscosity at 150°C for Series-I (left) and Series-II (right). Points - experimental, lines-computed.

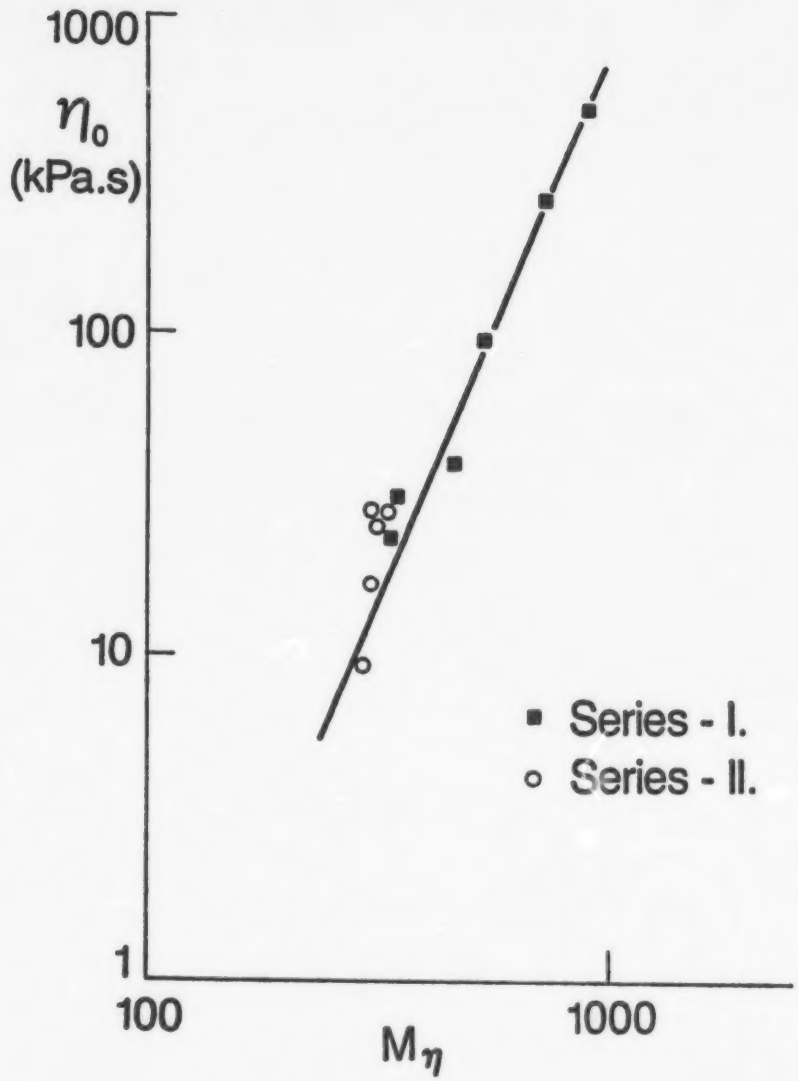

Fig. 7. Molecular weight dependence of the zero-shear viscosity for Series-I and II. The line represents the dependence for neat LLDPE resins (45).

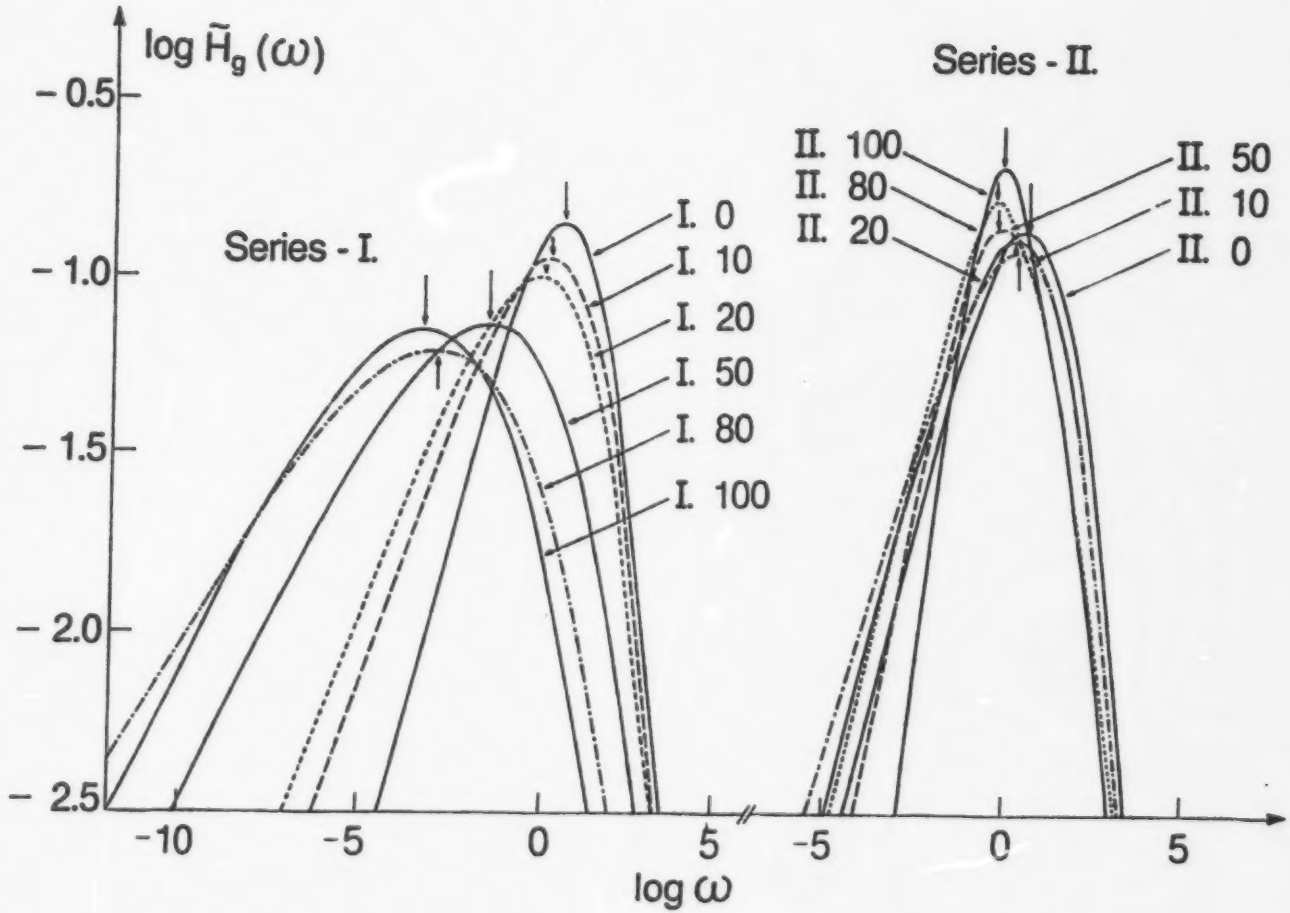

Fig. 8. Reduced frequency relaxation spectrum for Series-I and II. The arrows indicate computed coordinates of the maximum ($\tilde{H}_{G\ max}\ \omega_{max}$).

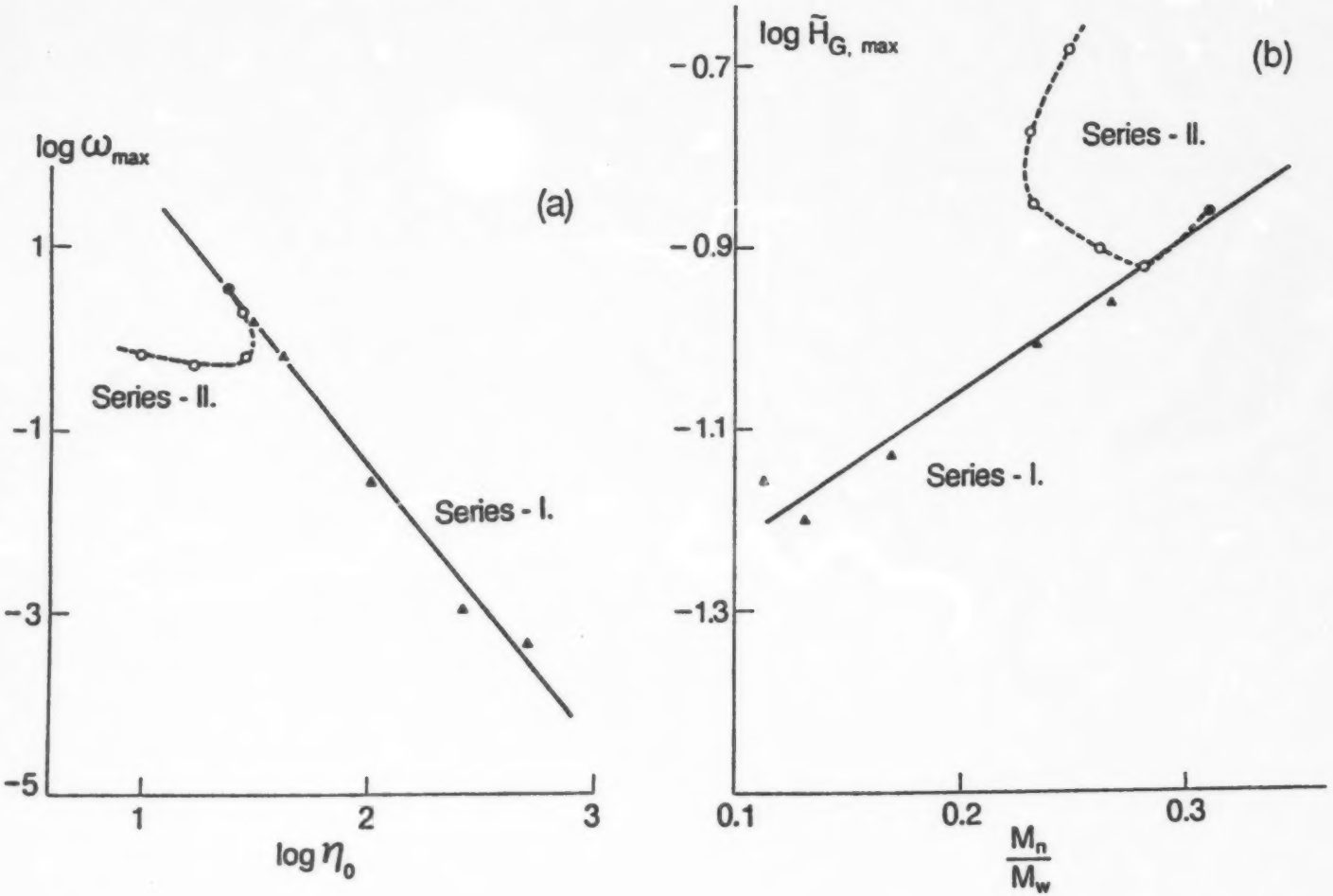

Fig. 9. a) Correlation between the abscissas of relaxation spectrum maximum and the zero-shear viscosity for Series-I and II; b) Correlation between the ordinate of relaxation spectrum maximum and the polydispersity factor M_n/M_w.

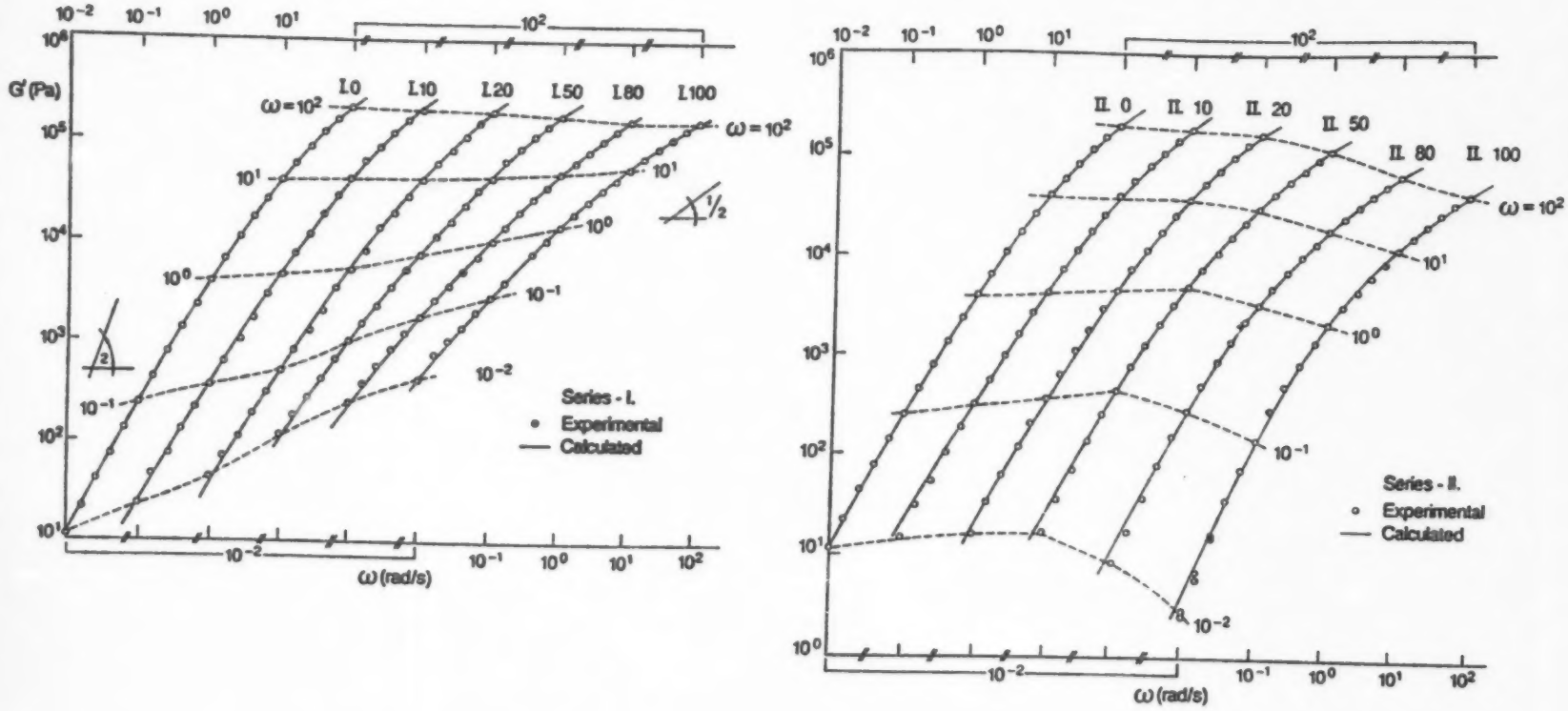

Fig. 10. Storage modulus vs. frequency for Series I LLDPE/LLDPE (left) and for Series-II LLDPE/LDPE blends (right) at 190°C. Points - experimental, solid lines computed from $H_G(\omega)$, broken lines connect the constant - ω data points. Concentration of the second component is given in wt%. The results for each blend is displaced horizontally by one decade.

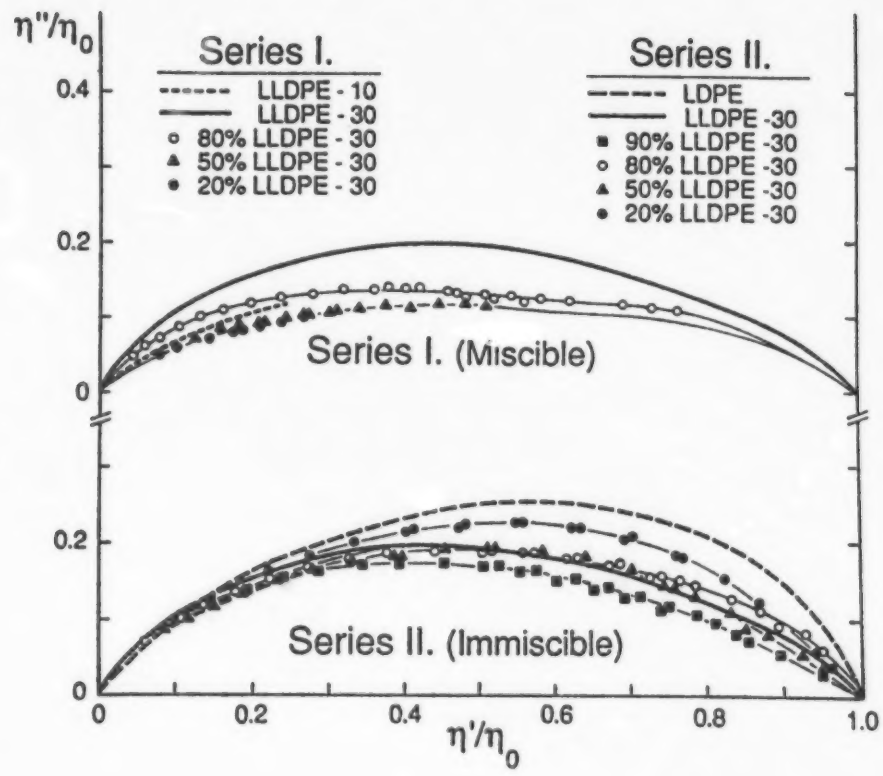

Fig. 11. Cole-Cole plot for miscible (Series-I) and immiscible (Series-II) polyethylene blends.

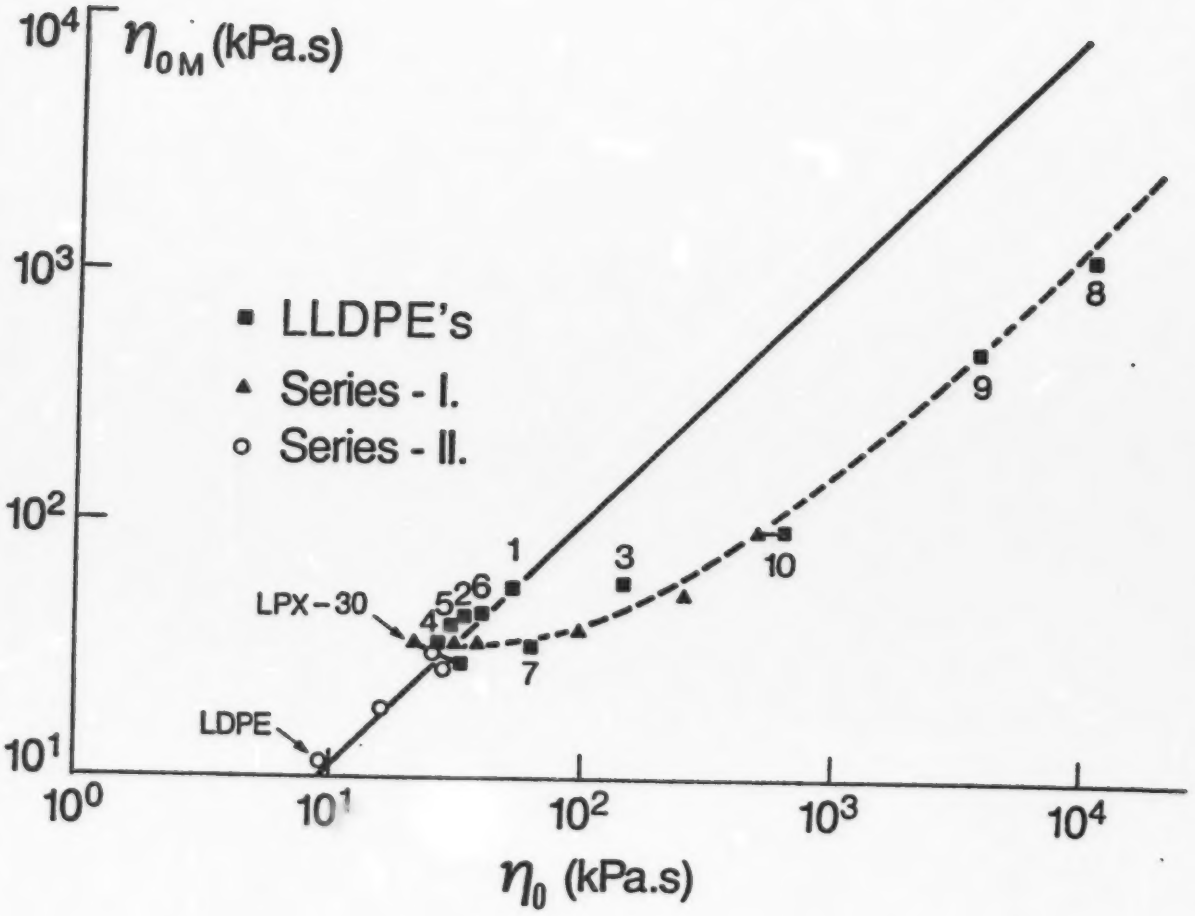

Fig. 12. Maxwellian zero-shear viscosity computed from cross-point coordinaters versus η_0 for Series-I and II as well as for neat LLDPE resins.

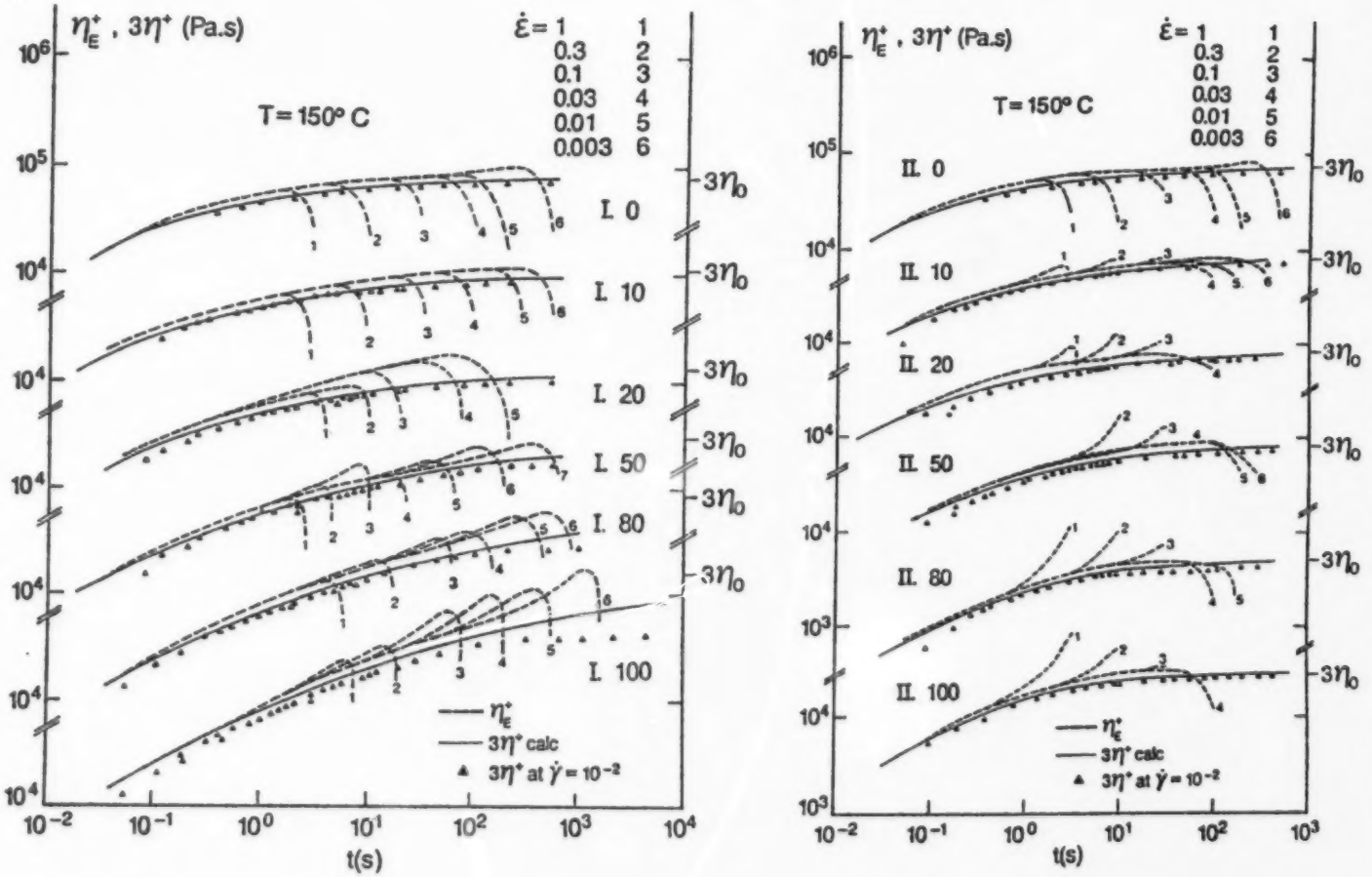

Fig. 13. Stress growth function for blends of linear low density polyethlene, LLDPE, with (A) another type of LLDPE (miscible, Series-I) and (B) with low density polyethylene (immiscible, Series II). The broken lines represent experimental data in elongation, the triangles indicate experimental data in steady state shearing at $\dot{\gamma} = 0.01s^{-1}$. The solid lines were computed from the relaxation spectrum (14).

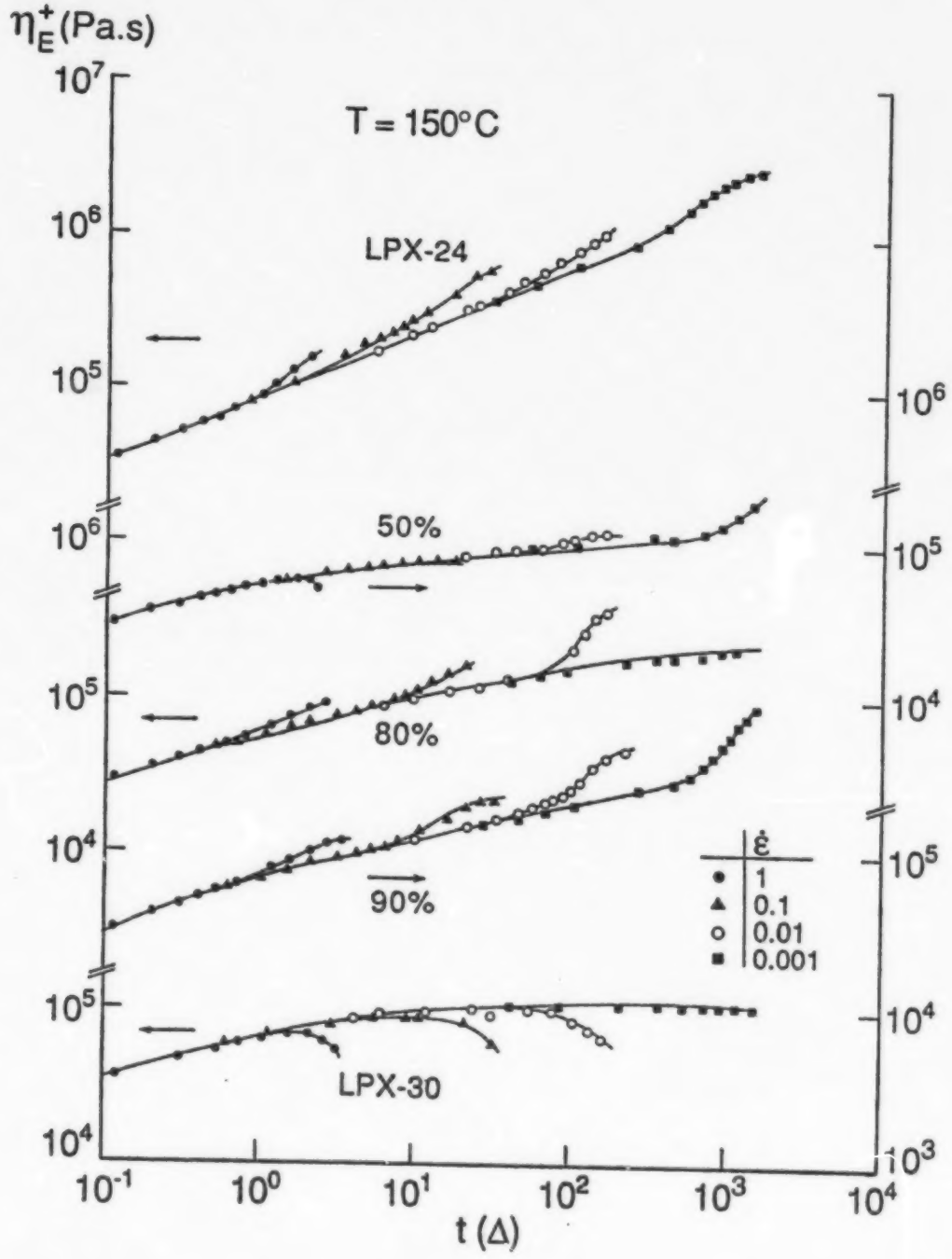

Fig. 14. Stress growth function in uniaxial extension vs. time for LPX-30/LPX-24 blends (Series-III) at T=150°C and $\dot{\varepsilon}$ = 0.001,0.01, 0.1 and 1 (s^{-1}).

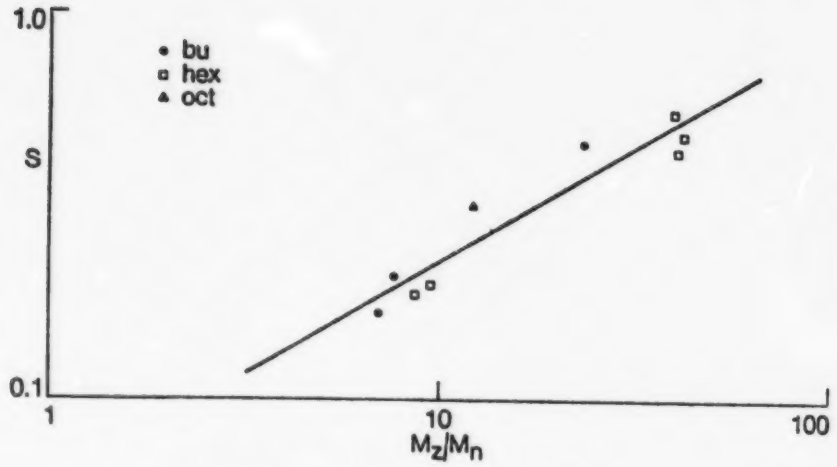

Fig. 15. Initial slopes of the stress growth functions of LLDPE's (containing butene, hexene or octene comonomer) as function of resin polydispersity.

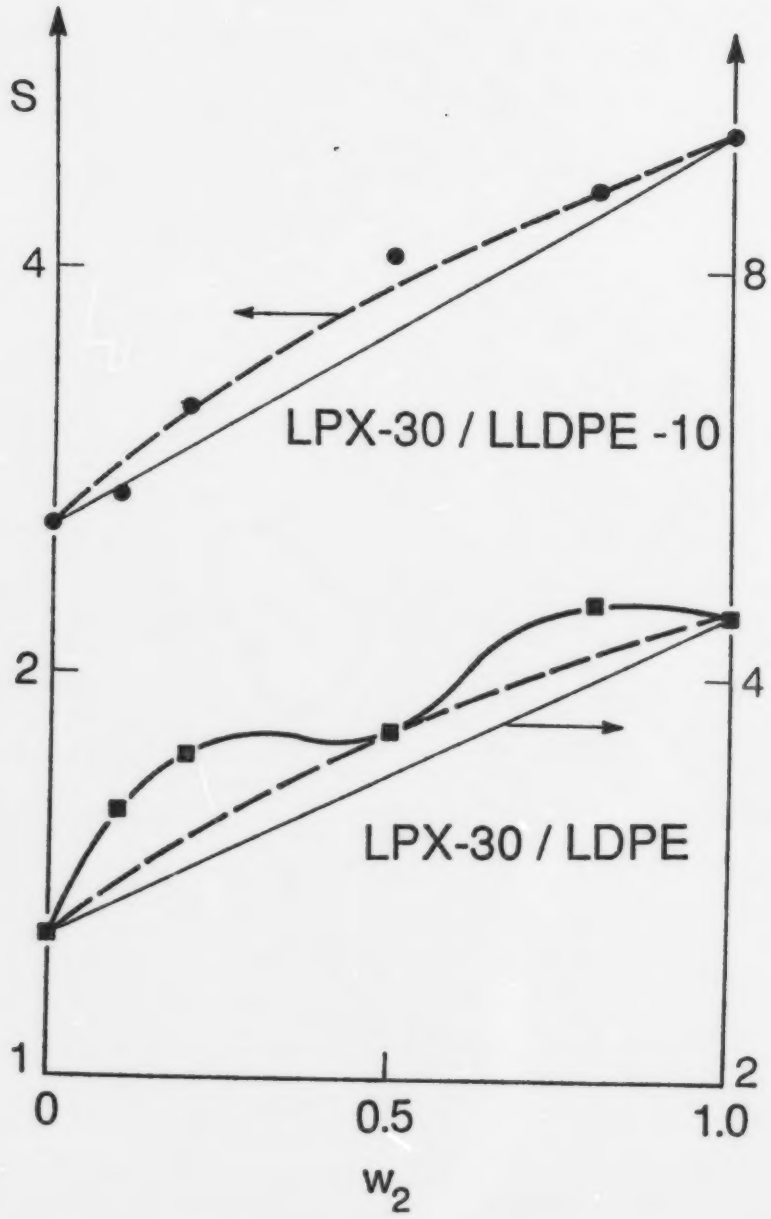

Fig. 16. Compositional dependence of the initial slope of the elongational stress growth function for LPX-30/LLDPE 10 (top) and LPX-30/LDPE (bottom). The broken lines were computed assuming miscibility.

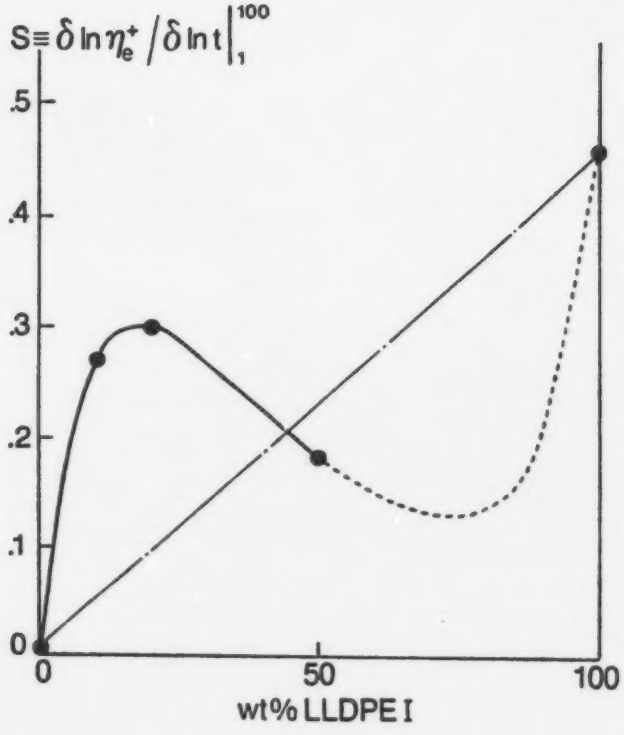

Fig. 17. Initial slope of the stress growth function for LPX-30/LPX-24 blends vs. composition.

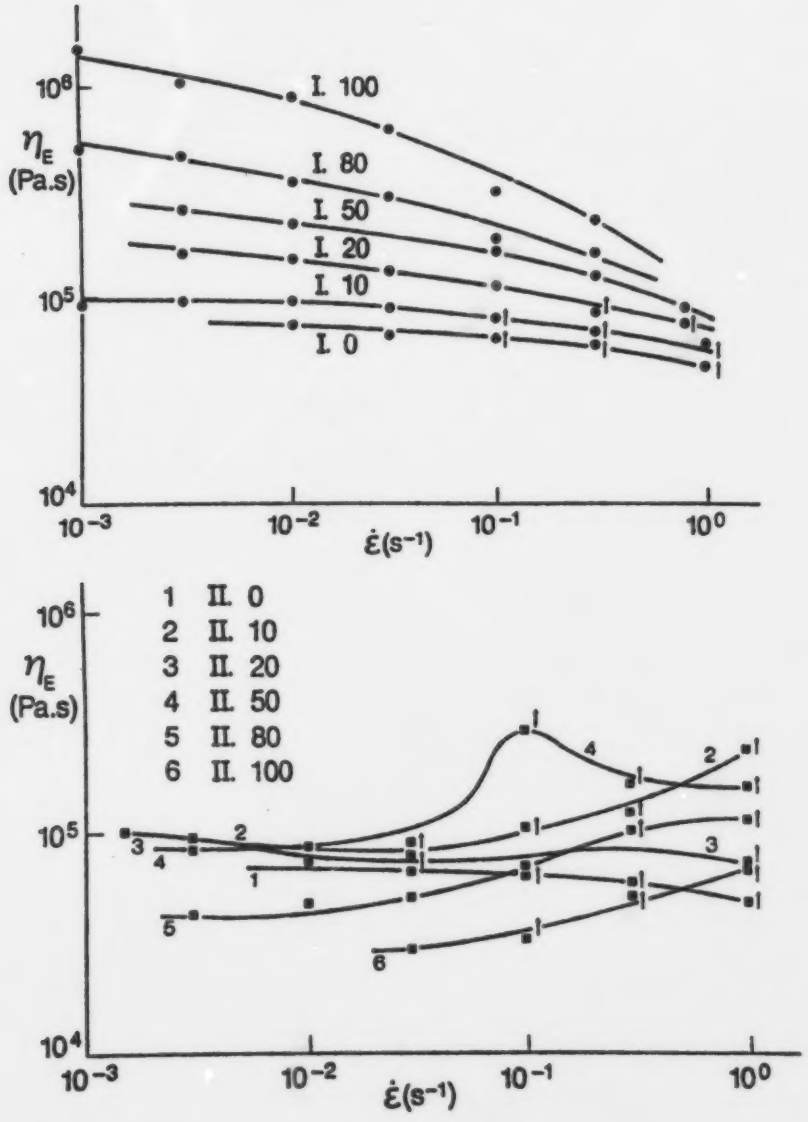

Fig. 18. The elongational viscosity in steady state flow at T = 150°C vs. strain rate for Series-I LPX-30/LLDPE-10 blends (top) and Series-II, LLDPE/LDPE blends (bottom). The data points marked with arrow on a side indicate that equilibrium value has not been reached.

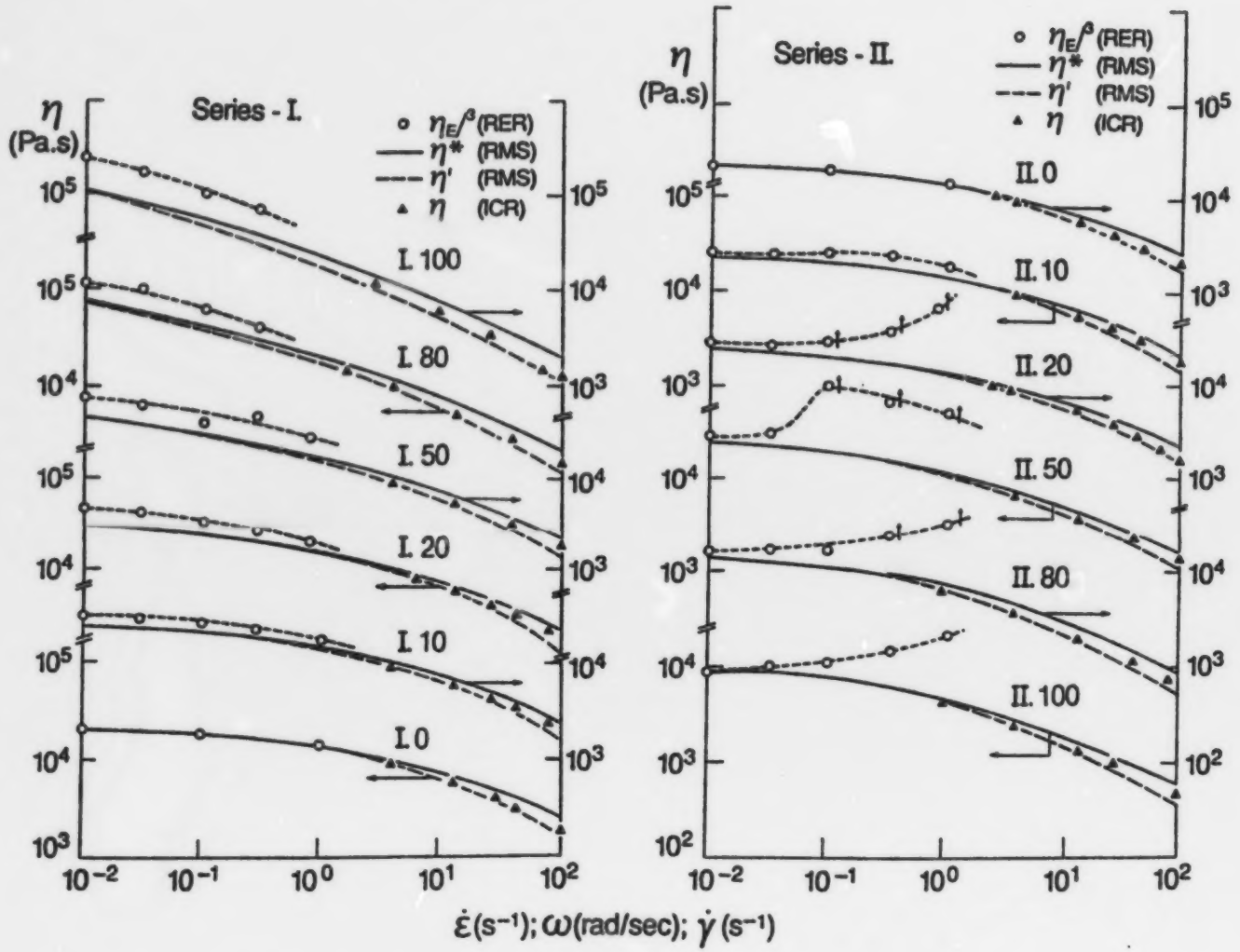

Fig. 19. Comparison of rate of deformation dependence of the steady state (capillary) viscosity, η, (points) with the complex, η*, (solid line) dynamic, η', (broken line) and extensional viscosity, $\eta_E/3$ (open circles). The data are reduced to common temperature 150°C. Left, Series-I, LLDPE/LLDPE, right Series-II LLDPE/LDPE blends. For clarity, the data of each blend is vertically displaced by one decade.

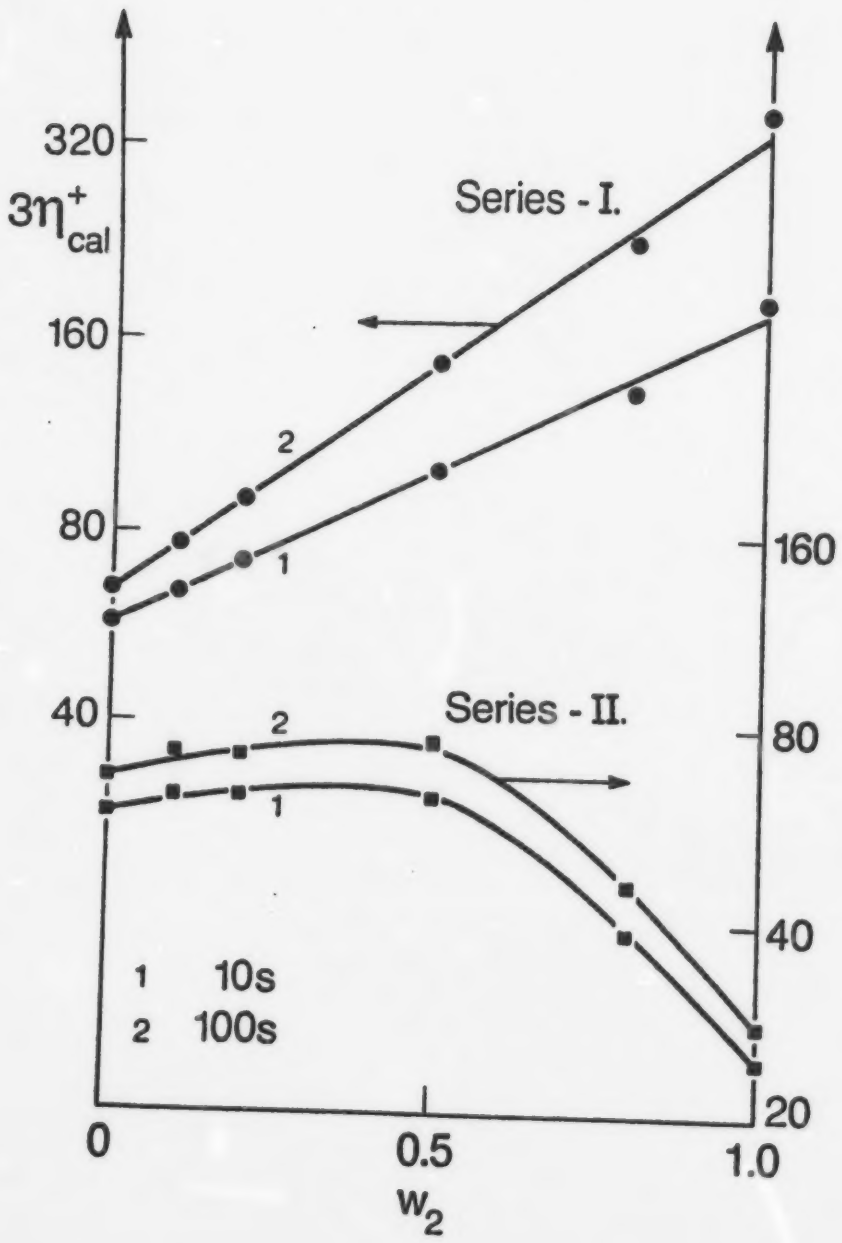

Fig. 20. Compositional dependence of $3\eta^+_{calc} = \eta^+_{E,lin}$ at t = 10 and 100(s) for Series-I (top) and Series-II (bottom).

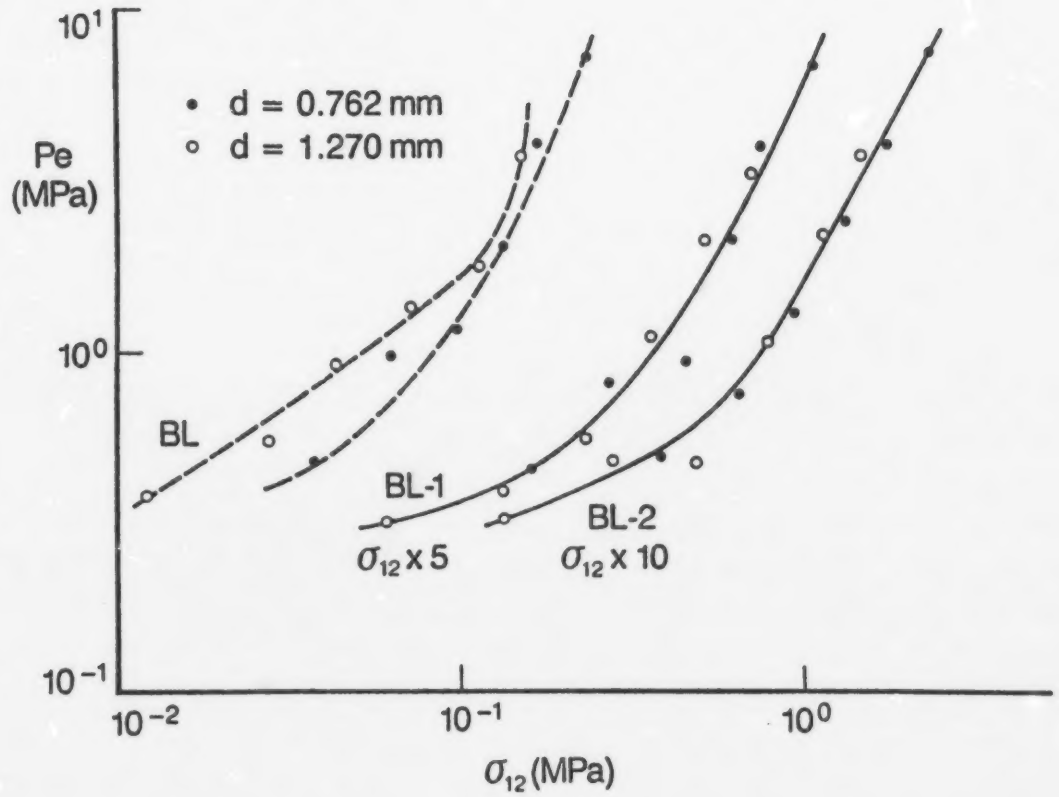

Fig. 21. Bagley pressure correction term, Pe, versus shear stress, σ_{12}, for BL, BL-1, and BL-2. Data for BL-1 and BL-2 have been displaced horizontally by a factor of 5 and 10 respectively.

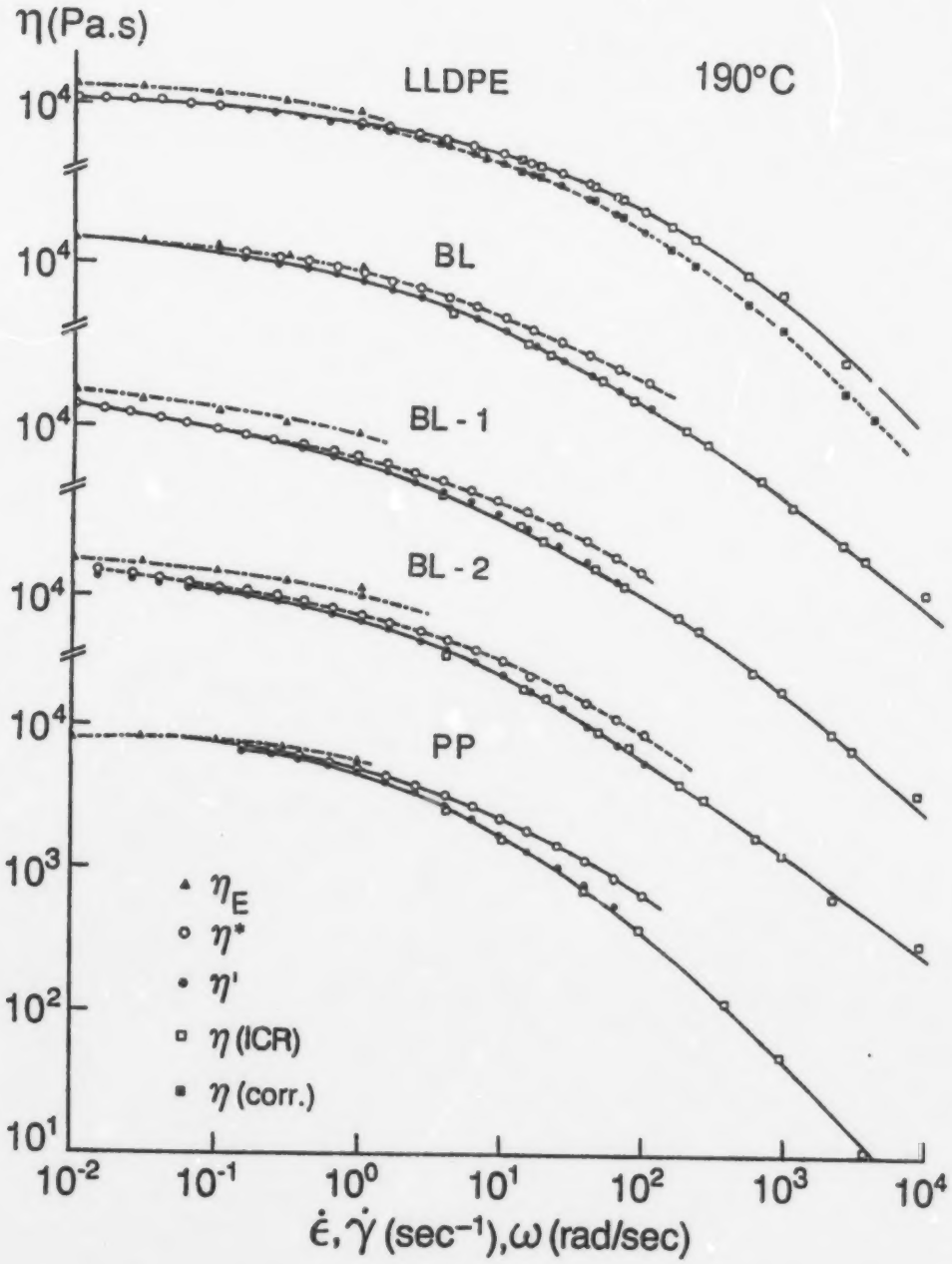

Fig. 22. Elongational, η_g, complex, η^*, dynamic, η', and shear, η, viscosities versus strain rate, $\dot{\epsilon}$, frequency, ω, or shear rate, $\dot{\gamma}$, for (from the top): LLDPE, BL, BL-1, BL-2 and PP at 190°C. The data corrected for pressure effects are shown as full squares. For clarity the traces are displaced vertically each by one decade.

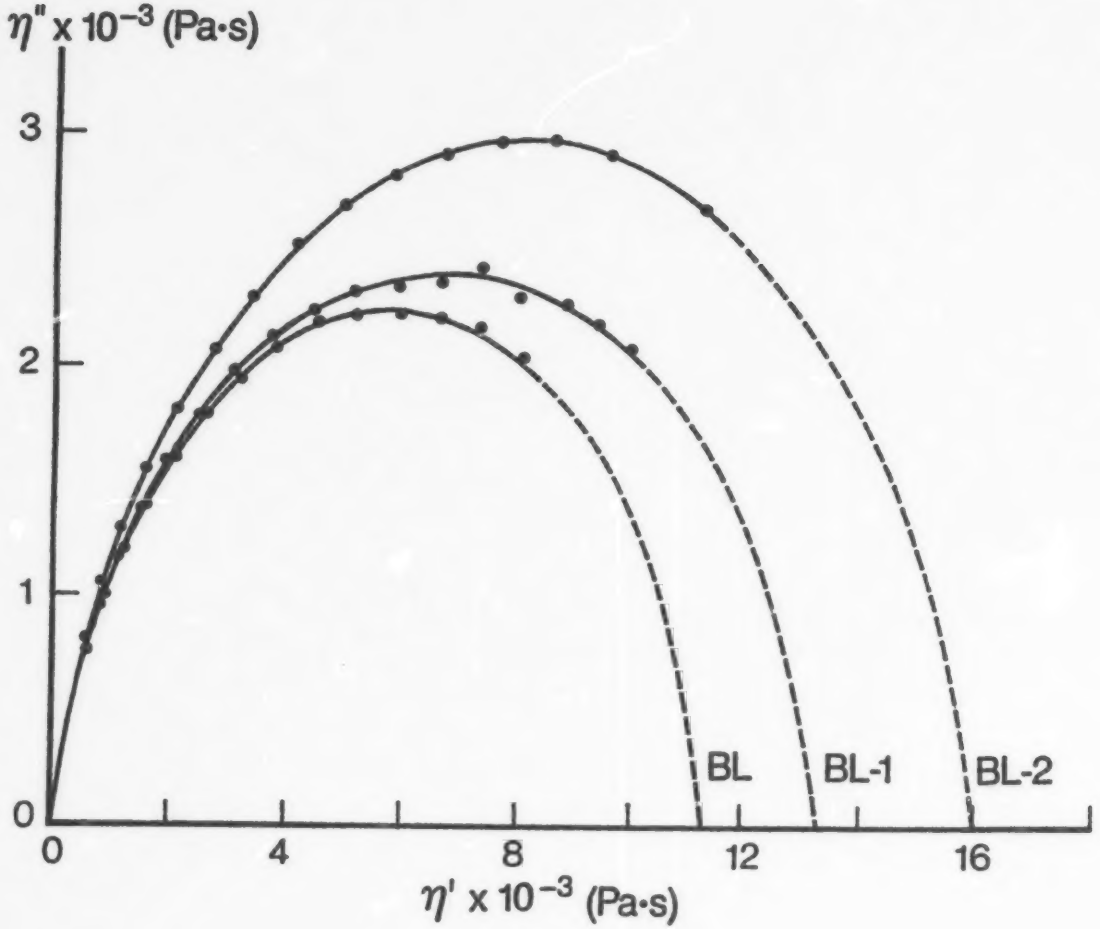

Fig. 23. Imaginary part, η", versus real part, η', of the complex viscosity for BL, BL-1, and BL-2.

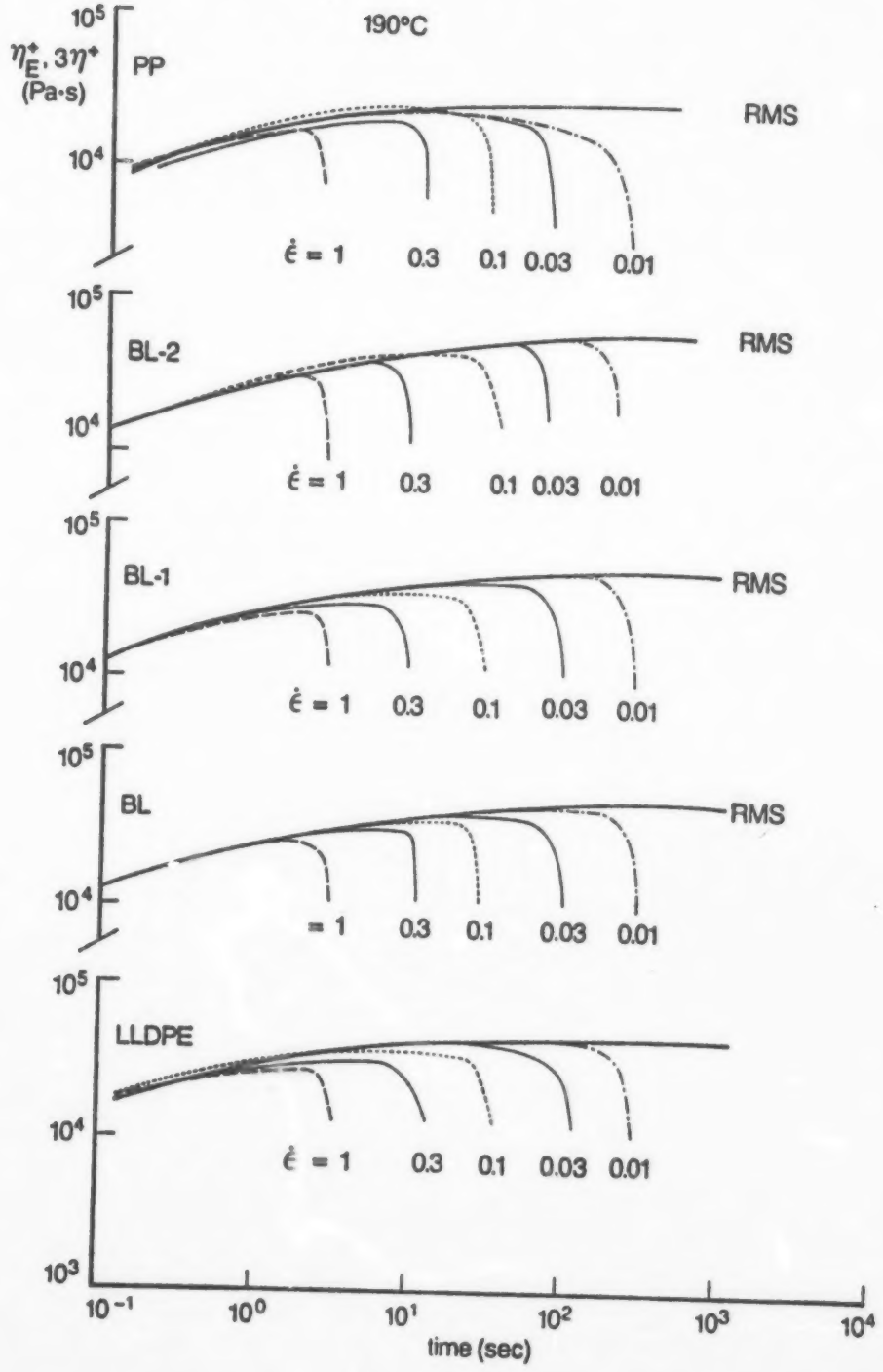

Fig. 24. Comparison of shear, $3\eta^+$, and elongational, η_E^+ time dependent viscosities for PP, BL-2, BL-1, and LLDPE at 190°C.

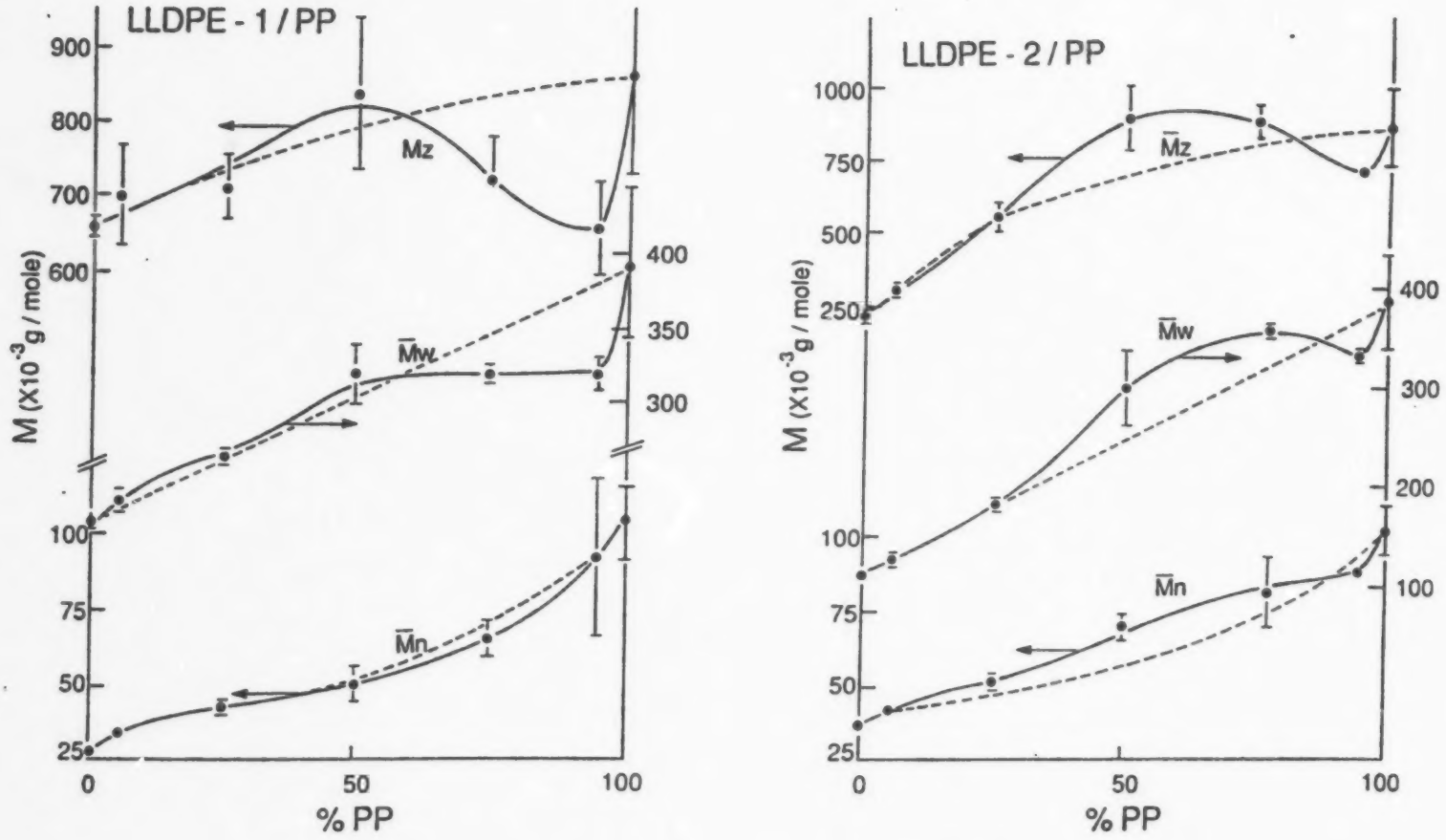

Fig. 25. Compositional variation of average molecular weights for System 1 (left) and 2. Points - experimental, broken lines - calculated.

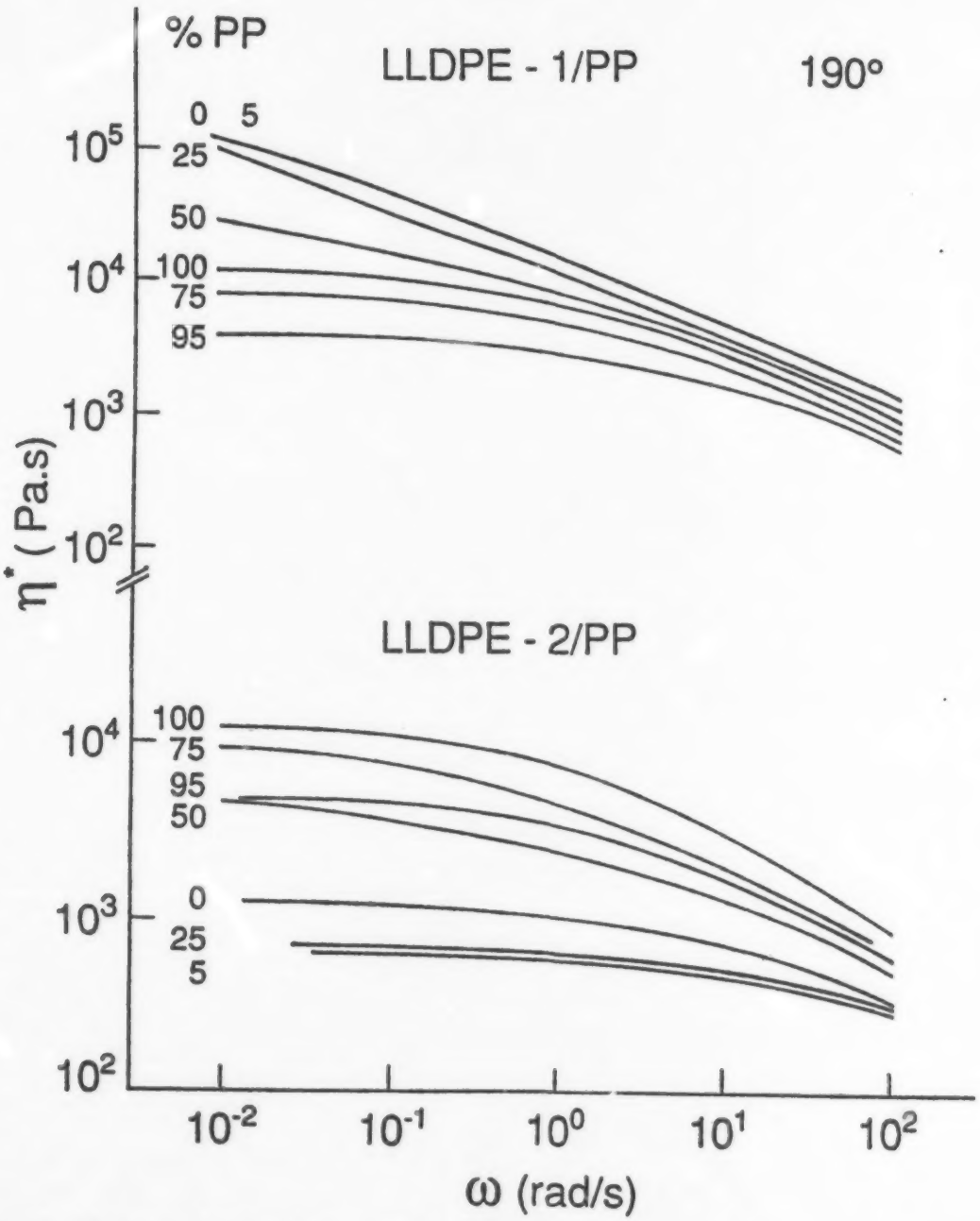

Fig. 26. Complex viscosity vs. frequency, η^* vs. ω, for System 1 (top) and 2. Points are experimental, lines computed from the relaxation spectrum.

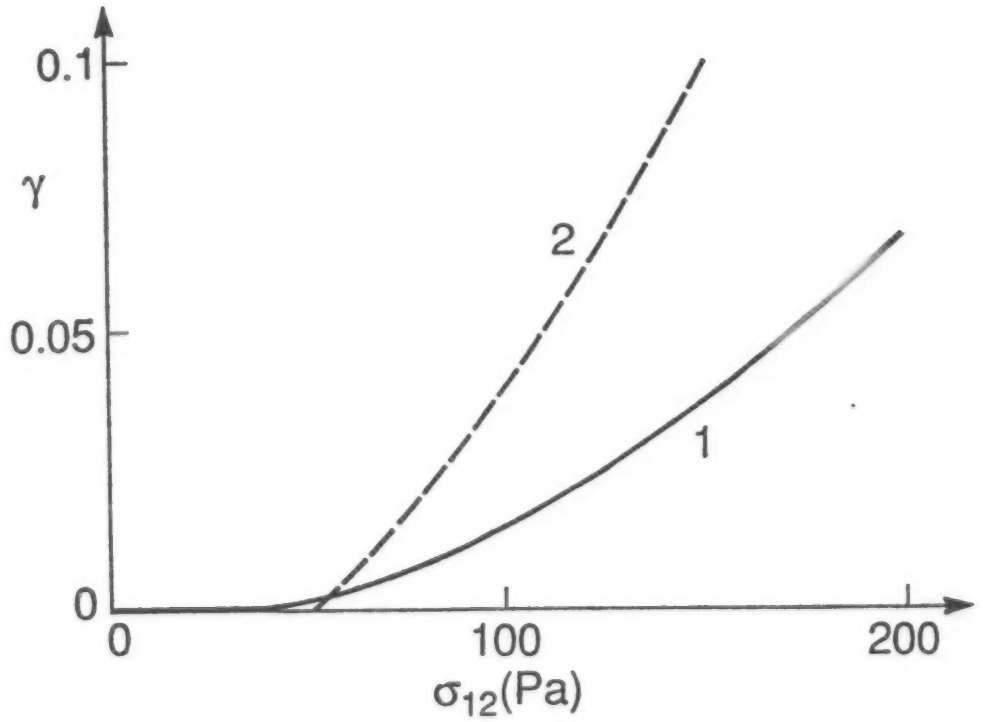

Fig. 27. Shear strain, γ, as a function of shear stress, σ_{12}, for blends containing 50% of each polymer. Curve 1: PP/LLDPE-1, curve 2: PP/LLDPE-2

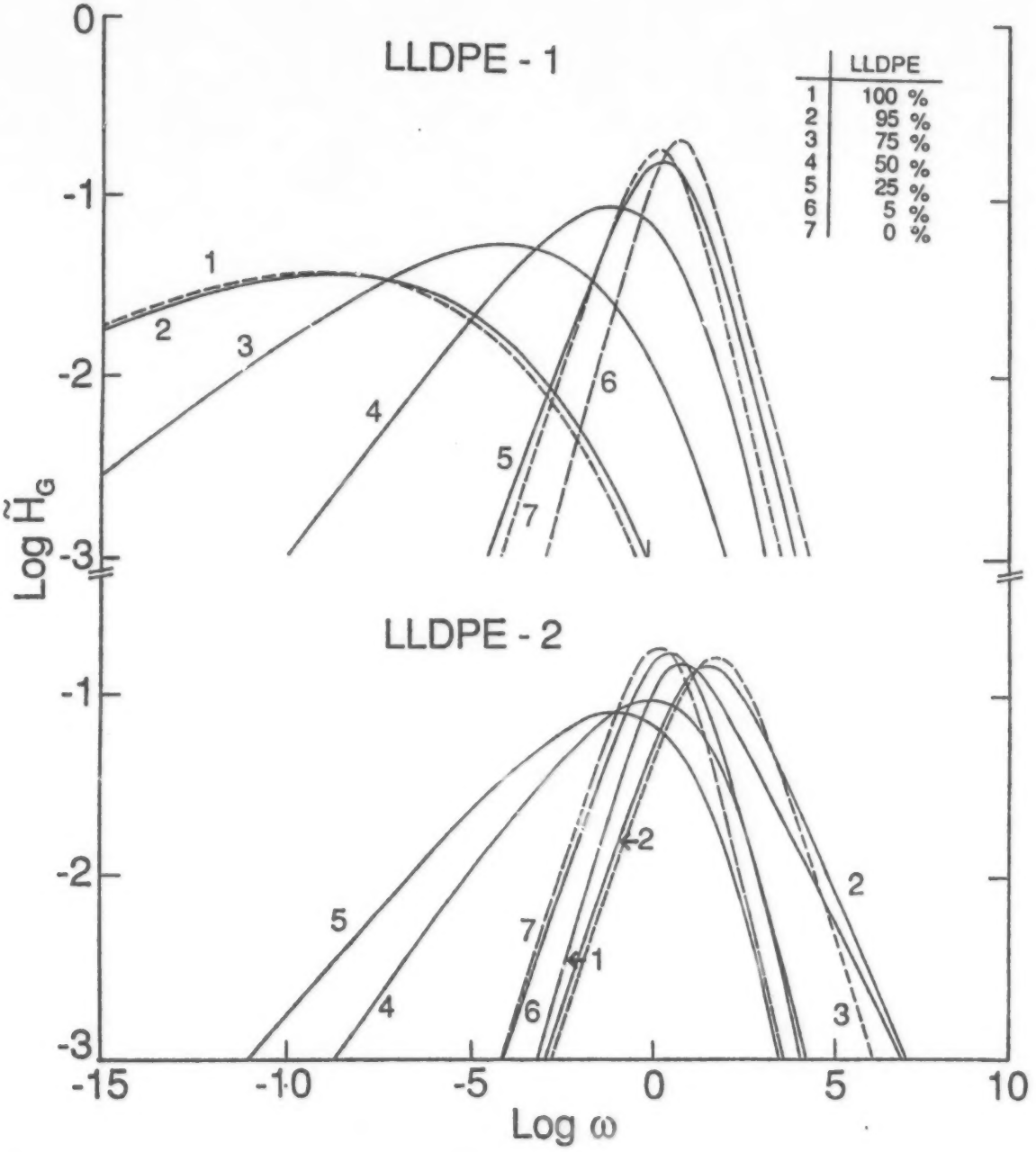

Fig. 28. Reduced frequency relaxation spectrum for System 1 (top) and System 2.

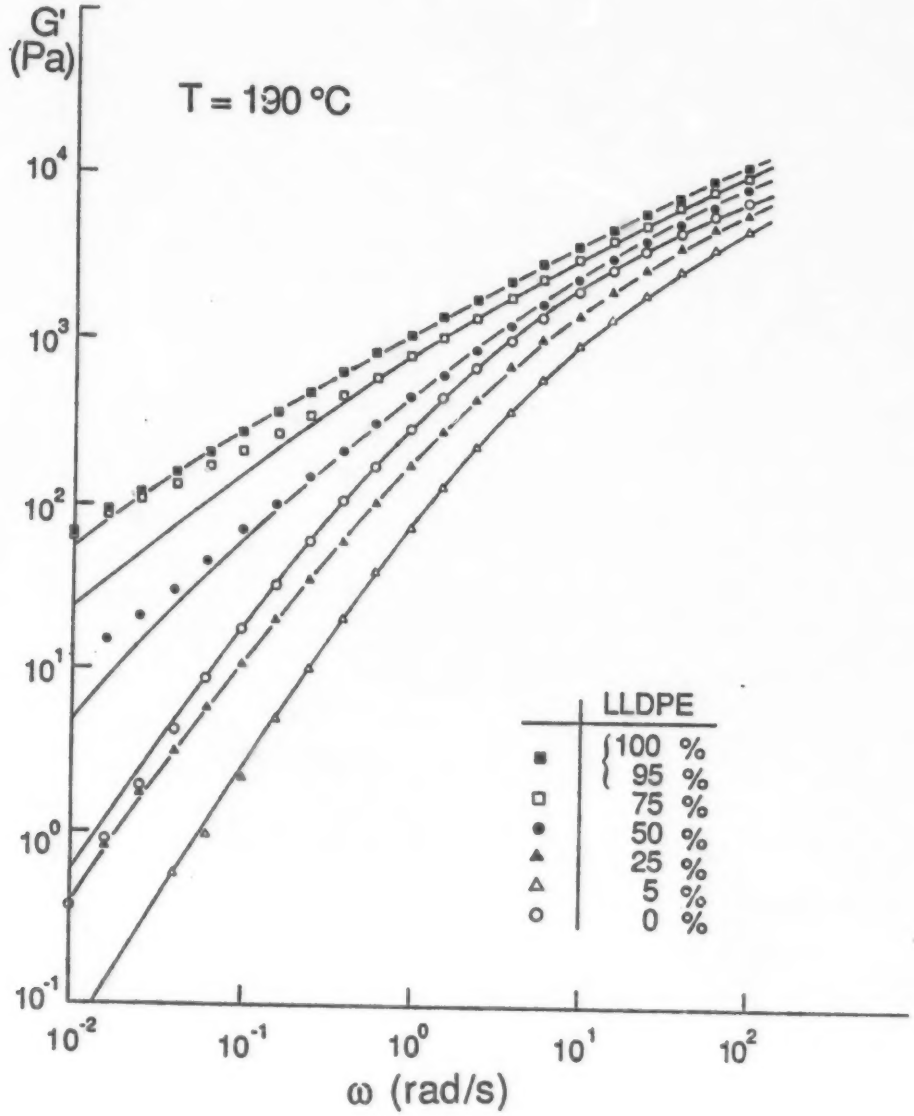

Fig. 29. Storage shear modulus vs. frequency, G' vs. ω, for System 1. The points are experimental, uncorrected for the apparent yield stress, the lines computed from the relaxation spectrum.

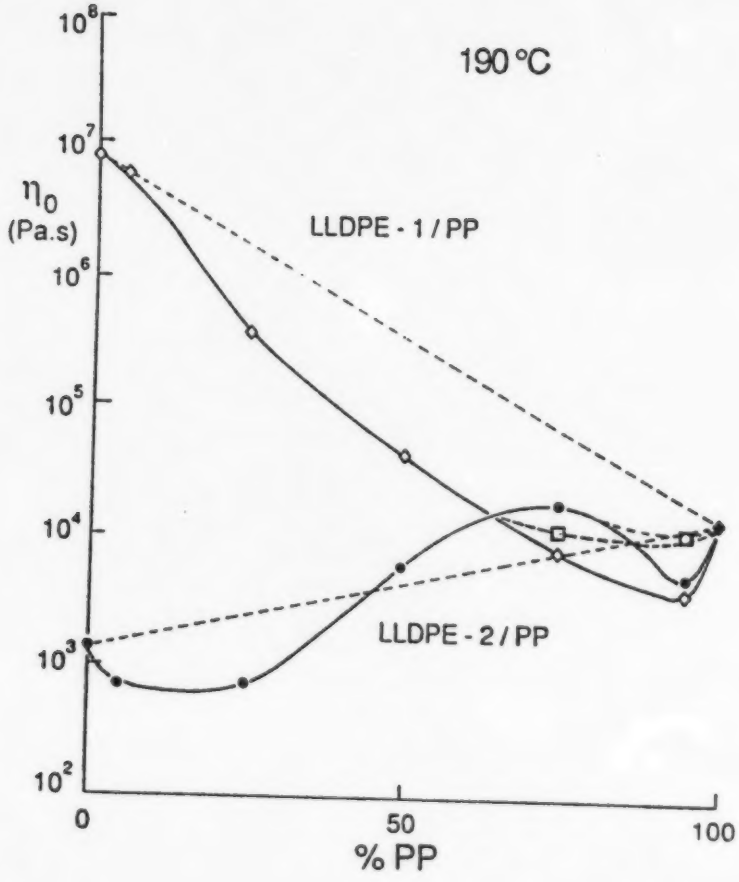

Fig. 30. Zero shear viscosity, η_0, vs. PP content in Systems 1 and 2.

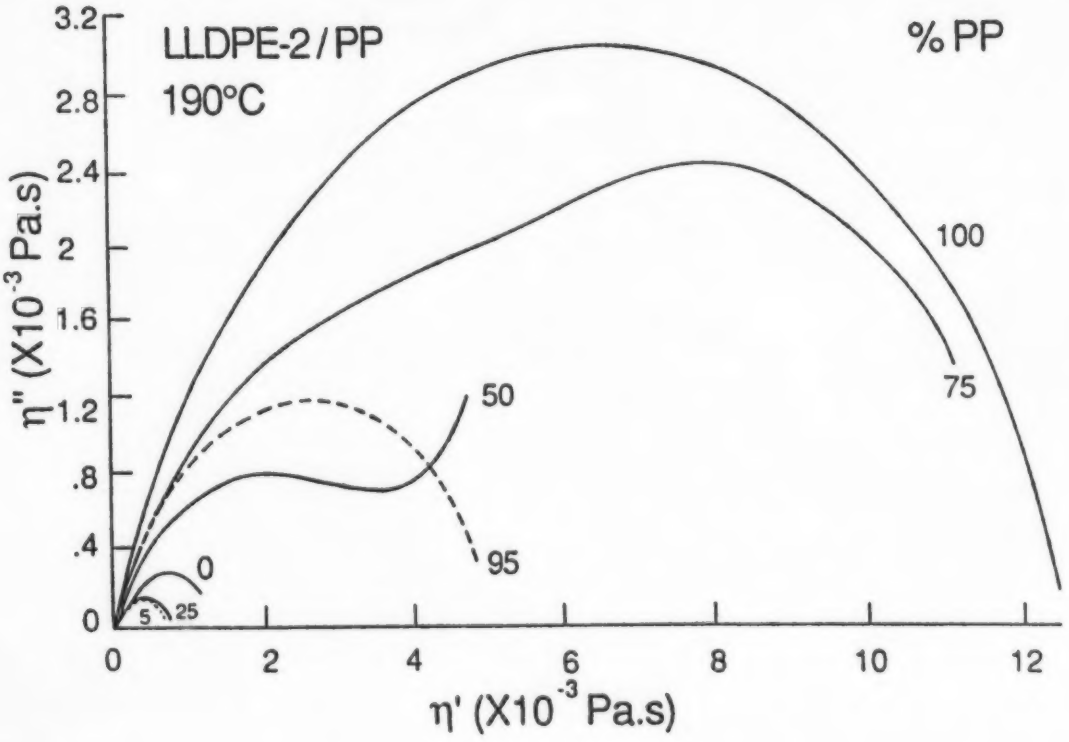

Fig. 31. Cole-Cole plot, η" vs. η', for System 2.

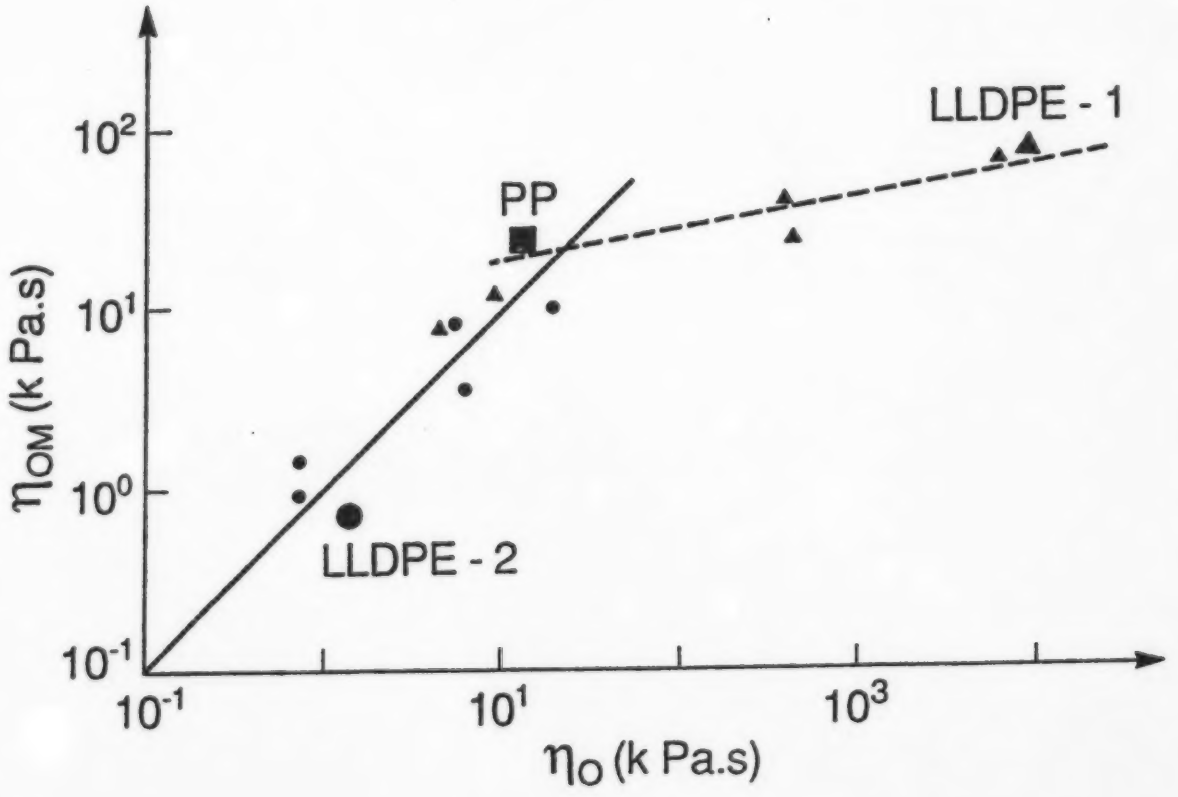

Fig. 32. Maxwellian viscosity vs. zero-shear viscosity for Systems 1 and 2.